HHS Public Access

Author manuscript

NMR Biomed. Author manuscript; available in PMC 2022 May 01.

Published in final edited form as:

NMR Biomed. ; : e4309. doi:10.1002/nbm.4309.

Advanced magnetic resonance spectroscopic neuroimaging: Experts' consensus recommendations

Andrew A. Maudsley[1], **Ovidiu C. Andronesi**[2], **Peter B. Barker**[3], **Alberto Bizzi**[4], **Wolfgang Bogner**[5], **Anke Henning**[6,7], **Sarah J. Nelson**[8,†], **Stefan Posse**[9], **Dikoma C. Shungu**[10], **Brian J. Soher**[11]

[1]Department of Radiology, Miller School of Medicine, University of Miami, Miami, Florida, USA [2]Department of Radiology, Massachusetts General Hospital, Athinoula A. Martinos Center for Biomedical Imaging, Harvard Medical School, Boston, Massachusetts [3]The Russell H. Morgan Department of Radiology and Radiological Science, The Johns Hopkins University School of Medicine, and the Kennedy Krieger Institute, F.M. Kirby Center for Functional Brain Imaging, Baltimore, Maryland [4]Fondazione IRCCS Istituto Neurologico Carlo Besta, Milan, Italy [5]High Field MR Center, Department of Biomedical Imaging and Image-guided Therapy, Medical University Vienna, Vienna, Austria [6]Max Planck Institute for Biological Cybernetics, Tübingen, Germany [7]Advanced Imaging Research Center, University of Texas Southwestern Medical Center, Dallas, Texas [8]Department of Radiology and Biomedical Imaging, University of California San Francisco, San Francisco, California [9]Department of Neurology, University of New Mexico, Albuquerque, New Mexico [10]Department of Neuroradiology, Weill Cornell Medical College, New York, New York [11]Department of Radiology, Duke University Medical Center, Durham, North Carolina

Abstract

Magnetic resonance spectroscopic imaging (MRSI) offers considerable promise for monitoring metabolic alterations associated with disease or injury; however, to date, these methods have not had a significant impact on clinical care, and their use remains largely confined to the research community and a limited number of clinical sites. The MRSI methods currently implemented on clinical MRI instruments have remained essentially unchanged for two decades, with only incremental improvements in sequence implementation. During this time, a number of technological developments have taken place that have already greatly benefited the quality of MRSI measurements within the research community and which promise to bring advanced MRSI studies to the point where the technique becomes a true imaging modality, while making the traditional review of individual spectra a secondary requirement. Furthermore, the increasing use of biomedical MR spectroscopy studies has indicated clinical areas where advanced MRSI methods can provide valuable information for clinical care. In light of this rapidly changing technological environment and growing understanding of the value of MRSI studies for biomedical studies, this article presents a consensus from a group of experts in the field that reviews the state-of-the-art for clinical proton MRSI studies of the human brain, recommends

Correspondence Andrew Maudsley, Department of Radiology, Miller School of Medicine, University of Miami, 1150 NW 14th Street, #713, Miami, FL33136, USA. amaudsley@miami.edu.

†Died April 3, 2019

minimal standards for further development of vendor-provided MRSI implementations, and identifies areas which need further technical development.

Keywords

brain; magnetic resonance spectroscopic imaging; review

1 | INTRODUCTION

The combination of magnetic resonance spectroscopy with spatial encoding methods enables spectral information to be mapped in a noninvasive manner. Proton MR spectroscopic imaging (MRSI) has been of particular value for in vivo measurements in the brain, for both clinical and biomedical research studies.[1,2] Although proposed over 30 years ago[3-5] and widely implemented on commercial MRI systems, the clinical adoption of MRSI remains limited for reasons that include long acquisition times, low spatial resolutions, variable quality, inadequate analysis software and a lack of appreciation in the clinical community of the potential impact on clinical care. However, recent technological developments promise to transform MRSI into a more reliable and higher throughput modality through the increased availability of higher magnetic fields (≥3 T), multichannel detector systems, new encoding methods and new approaches for obtaining metabolite maps over large brain volumes. These developments promise to bring the quality of MRSI to the point where the technique becomes a true imaging modality and the more traditional analysis of individual spectra becomes a secondary requirement. Complementary to these technological developments has been increased experience within the research community of the potential value of MRSI-detected metabolic biomarkers for clinical studies. With this background of an evolving technology and increased understanding of the potential of MRSI, this report aims to: (1) summarize the state-of-the-art acquisition and analysis methods and review the status of clinical applications; (2) make specific recommendations for minimum implementation standards that apply to all MRSI studies; (3) recommend particular areas where further development is needed to bring advanced MRSI methods into the clinical setting; and (4) propose future directions where advanced MRSI methods should be implemented as part of research and clinical imaging protocols.

Both MRI and MRS technologies have numerous options in the choice of acquisition methods and parameters, which can result in multiple tradeoffs between information content and implementation considerations. Together with an ongoing and steady rate of development, these characteristics present challenges to the development of a set of implementation recommendations. Instead, this report aims to identify broad categories of clinical applications and emerging translational research areas for which different spatial or spectral sampling capabilities are recommended. For example, some applications can make effective use of relatively simple spectroscopic acquisitions to generate a map of the choline to N-acetylaspartate ratio, suggesting that acquisition design considerations can focus on optimizing spatial resolution and acquisition times. By contrast, studies that aim to measure neurotransmitters or tumor-specific molecular markers require optimum spectral discrimination and sensitivity, while spatial sampling becomes a secondary consideration.

Therefore, an additional aim of this report is to summarize these application-specific considerations in the choice of MRSI methods selection.

Limitations of this report include that it considers methods that have already been demonstrated for in vivo human studies and for which there is reasonable expectation that these can be translated into clinical practice. Technologies such as hyperpolarized MRS and multinuclear detection are not considered. Considerations for ^{1}H MRSI studies at ultrahigh field (>7 T) are discussed; however, this also remains an area of active development.

2 | CLINICAL UTILITY OF MRSI OF THE BRAIN

2.1 | Clinical applications

Despite the clear diagnostic potential of ^{1}H MRS and decades of effort demonstrating that it provides complementary information relative to MRI, it largely remains an investigational tool that is not recommended for reimbursement in several countries. As an “imaging” method, MRSI offers greater promise for routine clinical use than single voxel spectroscopy (SVS), although at the expense of increased measurement complexity and typically longer acquisition times. While a direct comparison of the clinical value and reliability of MRSI relative to SVS may not be possible, it is known that the limited spatial sampling of SVS methods can impact diagnostic value.[6,7] The typically smaller voxel volumes of MRSI have also been shown to enable sampling of brain regions where SVS results were of poor quality,[8] and while motion artifacts may be visible in MRSI, these can equally affect SVS measurements but without being apparent in the result.[9]

The spectral sampling in most MRSI studies is comparable with that used for SVS, so in principle MRSI can provide the same spectroscopic information as SVS, although acquisitions are typically designed to sample smaller voxel volumes, which reduces detection sensitivity[10] (signal-to-noise ratio [SNR] per unit time). As a result, most clinical studies using MRSI have focused on detection of prominent spectral components, namely, N-acetylaspartate (NAA), creatine (Cr) and choline (Cho) compounds, followed by a smaller number of studies that also include lactate (Lac), myo-inositol (mI) and the combined signal from glutamate and glutamine (Glx). Lower spatial resolution MRSI studies have also been demonstrated for detection of compounds that can be challenging even for SVS measurements, such as γ-aminobutyric acid (GABA)[11,12] and glutathione (GSH).[13]

An obvious benefit of MRSI over SVS for clinical applications is that spectra are obtained from multiple regions in a single study, which particularly benefits studies of heterogeneous pathologies. The following sections review clinical applications that particularly benefit from the multi-voxel sampling provided by MRSI.

2.1.1 | Brain tumors—Many brain tumors exhibit considerable heterogeneity and may have multi-focal lesions, making MRSI useful for identifying regions of infiltrative tumor[14-18] and guiding biopsy localization.[19-24] There is long-standing interest in the use of MRSI for treatment planning,[25-31] for which the widely reported metabolic changes that occur outside of MRI-observed abnormalities may have a significant impact on outcomes.[26,32-34] Additional applications include assessment of treatment response,[35-39] identifying

recurrent tumor,[40,41] and stratifying patients into subgroups for outcome assessments.[36] These applications benefit from having metabolic information over a large region and volumetric measurements are particularly beneficial.[41-45] Most studies are based upon the observation of increased Cho and decreased NAA in tumor tissue (Figure 1),[46] with improved contrast between normal and tumor tissue at longer TEs.[47] Meta-analyses provide evidence that Cho/NAA is effective for distinguishing high and low grade glioma and for separating regions with high grade pathology from areas of necrosis and less malignant tumor, although large variations in these findings have also been reported.[16-18] There is also increasing interest in making use of the entire metabolic profile, including changes of lipid,[48] glutamate,[13] glutamine, alanine,[49] GSH,[50] mI[51] (Figure 1) and D-2-hydroxglutarate (2HG), which is a marker of oncogenic IDH mutation status.[52,53] Since oncogenic IDH mutations are only found within the tumor there is no background 2HG signal, presenting considerable potential for mapping tumor distributions to guide and monitor treatment.[13,48,50,51,54-56] Implementation of 2HG measurement for volumetric acquisitions has also been demonstrated (Figure 2).[54,57,58]

2.1.2 | Epilepsy—Presurgical evaluation of epilepsy remains challenging, typically requiring co-localizing information from multiple diagnostic tests, including structural and diffusion MRI, PET, EEG and MEG. MRSI has been shown to provide complementary information via detection of altered tissue metabolism in the local neighborhood of a seizure focus, primarily from the reduction of NAA. Long echo time studies have indicated reduced NAA compared with healthy controls, as well as abnormal metabolism in the limbic and subcortical regions.[59] Detection of neocortical epilepsy particularly benefits from the availability of whole-volume mapping due to the cortical location and limitations of prior localizing information to direct placement of a smaller imaging volume.[8,60] This application may also particularly benefit from increased spatial resolution provided at higher magnetic fields. A study at 7 T showed that a positive outcome was associated with the extent of resection of the region of abnormal NAA/Cr.[61] Other metabolites of interest are GABA and glutamate,[62] although diagnostic value for MRSI remains to be shown.

2.1.3 | Traumatic brain injury—Traumatic brain injury and chronic traumatic encephalopathy are characterized by widespread metabolic alterations that can occur remote from regions indicated by structural MRI-observed lesions or altered DTI measures,[63,64] therefore, given the limitations of other localizing information, wide FOV MRSI measurements are best suited for studies of TBI. These metabolic alterations vary with severity and time after injury,[65] with dominant findings being decreased NAA and increased Cho in the subacute phase that may persist for many years.[66,67] Several studies have demonstrated an association of MRS biomarkers with cognitive assessments,[63,68] although this association is not strong within the mild injury group, for which 15% to 30% of subjects will experience longer term postconcussion symptoms.[69] Longer TE measurements, with sampling of NAA and Cho, appear to be suitable for studies of TBI; however, further studies are needed to determine if other MRS biomarkers are of value and whether there are associations of the spatial distributions of altered metabolites with cognitive outcomes.

2.1.4 | Multiple sclerosis—Multiple sclerosis is associated with demyelination, remyelination, gliosis and axonal loss over multiple brain regions. While focal lesions are observed on structural MRI, it has been shown that there are also widespread metabolic alterations in normal-appearing brain tissue that are relevant for assessing disease progression.[70] More specifically decreased NAA and increased Cho, mI and Glu have been found in normal-appearing white matter (NAWM) and, inside the acute lesions, reduced NAA, GABA and Glu and elevated mI have also been detected in gray matter.[71] MRSI is thus able to localize changes in both lesions and normal-appearing brain tissue[72] and is valuable for serial evaluation of disease progression and response to therapy.[73,74] With the more widespread availability of ultrahigh field scanners, it is also possible to evaluate changes of GABA and GSH.[74,75]

2.1.5 | Mitochondrial disorders—Mitochondrial disorders are a clinically, morphologically and biochemically diverse group of energy metabolism disorders with a variety of causes, including genetic, physiological and environmental.[76] Diagnosis is complicated by varied etiopathophysiology, novel mitochondrial DNA mutations, and heterogeneity of the genotypes and phenotypes. Existing screening tests are effective for only a limited number of variants, are invasive, and/or may not provide the required information. Because metabolic changes associated with dysfunctional mitochondria are generally distinctive and brain tissue- or region-specific, MRSI measurements can aid in diagnosis and provide indices of disease progression and therapeutic response. Particularly sensitive markers of mitochondrial dysfunction that are of clinical utility are changes in NAA[77,78] and parenchymal and/or CSF lactate,[77-79] which is upregulated in mitochondrial dysfunction.

2.1.6 | Other potential applications—MRS has been widely used for studies of psychiatric disorders, pain disorders and neurodegenerative diseases; however, definitive clinical applications outside of the research arena, and the value of spatial information on metabolite distributions, remain elusive.[80-82] Continued interest remains in the extension to ultrahigh field (7 T) studies for measurements of glutamate, glutamine, GABA[11,12] and GSH,[83] for example for response assessment[84] and to provide objective criteria for studies of psychopathological and therapeutic mechanisms. Another topic of interest is the search for biomarkers that discriminate disease subtypes with different disease progression or therapy response.

Brain infection is a rare application where ^{1}H MRSI has already proven clinical impact. An additional succinate peak reflects bacterial metabolism and is paralleled by NAA decrease and lactate increase.

2.2 | Status of clinical acceptance

MRSI sequences provided by MRI systems manufacturers are largely based on older technologies and as a result many research groups have developed their own methods. These implementations have not been widely distributed within the clinical MR community and this has led to a lack of standardization and poor integration into the clinical workflow. Additional barriers to more widespread clinical adoption include a requirement for

specialized expertise for quality control and interpretation, and difficulties associated with obtaining reimbursement.

Several technical limitations must be addressed by the equipment manufacturers before advanced MRSI methods can be widely accepted within the clinical community. The most challenging is that some brain regions cannot be reliably sampled due to local B_0 inhomogeneities, which cannot be corrected by manufacturer-implemented B_0 shim system designs, a limitation that has become of greater importance as target volumes have increased. However, for full clinical acceptance there needs to be an expectation that pathologies within any brain region can be reliably sampled. A second requirement is that MRSI reconstruction, postprocessing and quantitative analysis will have to be fully automated and integrated into the clinical workflow, including robust quality control (see section 5.1). A further limitation remains relatively lengthy acquisition times, which can present challenges for clinical workflows. Additional effort is also required to ensure quantitative equivalence between scanners and to demonstrate reproducibility to support multi-center studies.

3 | DATA ACQUISITION METHODS

3.1 | Spectral acquisition methods

The selection of MRSI acquisition methods must first consider the required spatial and spectral information requirements and relative difficulties for acquiring that information. Intermediate to long TE (>50 ms) acquisitions with volume or slice selection provide spectra that are simple to interpret[85] and less susceptible to lipid contamination and baseline distortions, and therefore are preferred for whole-slice or whole-brain studies.[86] Short TE sequences are generally better suited for mapping J-coupled metabolites but must account for stronger lipid and macromolecular contributions.[87] PRESS or sLASER excitation sequences with sampling of the second half of a spin-echo is most widely implemented, although pulse-acquire FID acquisitions are being increasingly used for measurements at ≥7 T due to lower SAR requirements, while also increasing SNR due to minimal T_2-relaxation and J-evolution,[88,89] having negligible chemical shift displacement errors (CSDEs) and lower sensitivity to B_1 inhomogeneities.[90-92] Since FID-excitation requires a full-slice or whole-brain selection, this also requires effective control of extracranial lipid signal during image reconstruction[88,89,93-95] and careful handling of macromolecular signals.[96]

Sampling of metabolites at the lower limits of MRS detection (≤2 mM) or with strong spectral overlap (e.g. GABA, GSH) typically requires spectral editing and large voxels,[97] although implementations at high field strengths are changing the volume considerations.[98,99] The main obstacle for spectrally edited MRSI is the sensitivity to B_0 inhomogeneities and temporal frequency drifts, although three-dimensional (3D) MRSI implementations have been reported.[11,12,99]

3.2 | Spatial acquisition methods

3.2.1 | Volume selection and lipid removal—Primary acquisition considerations for brain MRSI include reduction of signal contamination from extracranial lipids, efficient

sampling of spatial k-space information to obtain the target spatial resolution and SNR within acceptable acquisition times,[100] and an ability to achieve the necessary B_0 homogeneity over the volume of interest (VOI). VOI excitation by PRESS, STEAM, semi-LASER or LASER[101] is commonly used to avoid extracranial regions,[102,103] although it has limitations of requiring positioning of the VOI and poor sampling of cortical regions. In addition, PRESS-based volume selection at higher fields leads to an unacceptably large CSDE.[103]

Full-slice or whole-brain excitations, as well as multi-slice MRSI with carefully tailored outer volume saturation (OVS),[104] improve the ability to investigate cortical regions and have the significant advantage that knowledge about the location of pathological abnormalities is not required. However, they face additional challenges with B_0 and B_1 field inhomogeneity that impact spatial or spectrally selective excitation or saturation methods. Whole-brain excitation has chiefly been combined with intermediate or long echo times to mitigate the lipid contamination and baseline problems, but this limits the number of metabolites and the achievable spatial resolution. Whole-brain coverage at medium and short TEs requires additional considerations for reduction of lipid signals. This may include OVS[105,106] or lipid inversion-nulling[107]; however, OVS requires automated placement procedures for clinical applications,[108,109] is SAR-demanding and difficult to implement for larger field of views (FOVs), and inversion-nulling incurs a loss of sensitivity, suppresses diagnostically relevant lipids, and still benefits from selective saturation of the orbits and fronto-temporal regions. Additional approaches include the use of specialized gradient coils for dephasing signals near the scalp[94,110] and relying entirely on higher spatial resolutions and optimization of the spatial response function (SRF), which can be done using acquisition,[79] reconstruction,[111-115] and postprocessing (see section 4) methods. For large VOI acquisitions, additional considerations include that a wide range of spectral quality is inevitably obtained, placing additional demands on quality control and spectral analysis. With the use of multichannel detection and increasing resolutions the sizes of the sampled volumetric raw data can become significant (~20-100 Gb), making rapid processing on current scanners challenging.

Typical spatial resolutions for 3 T measurements of the major singlet resonances and high abundance multiplets range from 0.3 to 1.0 cc with scan times of the order of 10 to 18 minutes.[91,113] With FID acquisition and constrained reconstruction methods, voxel sizes as small as 0.04 cc nominal voxel volume have been reported.[116,117] At 7 T, nominal voxel sizes of 0.023 cc have been reported using a FID acquisition method and scan time of 17 minutes.[118]

3.2.2 | MRSI encoding—Cartesian phase-encoded MRSI, often combined with elliptical k-space distribution, is the most commonly implemented acquisition strategy; however, for higher spatial resolutions this leads to long scan times. Several k-space undersampling methods such as parallel imaging, compressed sensing or multi-band encoding[119-121] have been demonstrated, with acceptable tradeoffs between data quality, scan time and spatial resolution, although with increased motion sensitivity and lipid fold-in artifacts for higher accelerations. Increased sampling efficiency can be obtained using spatial-spectral encoding (SSE) methods that combine sampling of spectral information with simultaneous sampling

along one or two k-space dimensions. Initially implemented using echo planar readout (EPSI),[87,122] several non-Cartesian trajectories have also been used.[112,123,124] These can also be combined with k-space undersampling and multi-band encoding to further increase sampling efficiency.[125-130] When implemented at higher field strengths these advanced MRSI methods can provide metabolite maps of relatively high spatial resolution within clinically acceptable acquisition times (Figure 3).[131] Limitations of these methods include increased noise, gradient heating leading to frequency drifts, more complex image reconstruction, and maintaining sufficient spectral bandwidth for ≥7 T, although temporal interleaves can be used to increase spectral sweepwidth.[132,133]

3.3 | Implementation considerations

3.3.1 | B_1 and B_0 inhomogeneity—Both intra-voxel and global B_0 homogeneity must be considered for MRSI. Intra-voxel inhomogeneity is dominated by local magnetic susceptibility variations, with strong effects in regions such as the temporal-frontal brain due to the tissue-air interface, or near hemorrhage, calcifications, or surgical cavities. Smaller voxels or spatial oversampling can be used to increase the volume over which suitable quality spectra can be obtained, although with a tradeoff with SNR.[134-136] For whole-brain studies at 3 T using spatial oversampling with a nominal voxel volume of 0.31 cc, the effect of intra-voxel inhomogeneity limits sampling to ~ 75% of the brain volume[137] although there is considerable variability between subjects and instruments. Global B_0 inhomogeneity, i.e. over the whole FOV, results in spatially dependent frequency shifts that can degrade frequency-selective water or lipid suppression, or spectral editing. Achieving an acceptable global B_0 homogeneity becomes increasingly difficult for larger FOVs and for whole-brain studies there is a high likelihood of large unsuppressed water or extracranial lipid signals, and metabolite signals close to water or lipid may be impacted. With current B_0 shim capabilities, frequency-selective spectral editing is therefore only recommended for centrally located volumes where global B_0 homogeneity can meet the strict requirements.

Image-based B_0 shim algorithms with robust convergence, spatial constraints and reliable calibration are required, together with suitable B_0 shim strengths.[138] Shim array coils,[139,140] high order shim systems[141] and dynamic B_0 shimming[93] promise to provide considerably improved performance; however, these are currently not supported by MRI manufacturers.

B_1 inhomogeneity leads to spatially dependent signal losses in metabolite images. These effects can be minimized by using sequences with B_1-insensitive or low flip angle pulses,[102,103] and can be corrected for by applying signal normalization (see section 5.2).

3.3.2 | Temporal instabilities—Subject motion results in image artifacts, decreased SNR and degraded SRFs. In addition, B_0 homogeneity is altered, meaning that a full correction of these effects requires real-time updates of the scanner frequency, gradients and B_0 shims. B_0 field drifts can be caused by gradient heating, particularly with the SSE methods,[142] or following gradient-intensive MRI sequences such as diffusion or fMRI.[143] If not corrected, these lead to degraded water suppression and cause problems with acquisition methods that include temporal interleaves or signal averaging.

3.3.3 | Reference measurements—Several of the artifacts mentioned in the previous sections can be addressed with one or more reference measurements. Motion correction can use methods described for MRI,[144] and real-time frequency correction can be implemented using a frequency navigator[145] or a full B_0 shim correction measurement,[146] which may increase the minimum TR. Implementation of both frequency drift and motion correction during the acquisition is highly recommended for clinical studies.

Separate water MRSI or MRI measurements can be used to support several processing functions. A water MRSI reference is the most convenient method for applying B_0 and lineshape corrections and signal normalization, similar to the approach widely used for SVS, and is strongly recommended. This can be acquired as a separate measurement performed with reduced TR and reduced k-space sampling to minimize the additional scan time,[147-149] while assuming the same head position, or as an interleaved measurement following the water-suppressed acquisition,[142] which lengthens the minimum TR time.

4 | MRSI PROCESSING METHODS

4.1 | Spatial reconstruction and spectral processing

Multichannel detection is routinely used to optimize sensitivity and enable parallel-imaging acceleration methods. The processing methods used for MRSI are similar to those widely implemented for MRI,[120,128,150-155] although they additionally require information on the phase of the detection sensitivity distributions.

Spectral processing for MRSI includes, as a minimum, the typical steps used in SVS, including removal of residual water, frequency/lineshape/phase correction (ECC) and Fourier transform. The spatial dimensions increase the data storage requirements, complexity and computation time relative to SVS processing, requiring 10s to 100s of minutes to process volumetric MRSI that may contain several thousand voxels.[86,87]

The limitations of detection sensitivity and spatial encoding efficiency (section 3.2) may result in low spatial resolutions and signal contamination due to the broad SRF, which can notably result in the propagation of extracranial lipid signals. These effects can be reduced using spatial smoothing, at the expense of reducing the effective spatial resolution, or weighted k-space acquisition.[131] Alternatively, image reconstruction approaches that control the SRF by incorporating a priori spatial information of the lipid regions,[156-158] or signal removal based on lipid spectral patterns,[157,159] can be applied.

Several noise reduction methods can be used to improve visual interpretation of metabolite images and spectra. Spatial smoothing and image interpolation can improve the appearance of metabolite images and noise reductions can be obtained from constrained spatial reconstructions.[117,160] When reporting acquisition parameters, the effective spatial resolution, ie the final value after smoothing, should be stated. Spectral filtering or denoising[161,162] can also be used to improve the appearance of spectra, although apodization-smoothing should be kept to small values (e.g. ≤2 Hz at 3 T) so as not to impact the accuracy of the spectral analysis. However, in this regard, the contrast in MRSI metabolite maps is commonly of greater importance than quantitation accuracy.

4.2 | Spectral fitting

Given the large number of spectra in MRSI data, fully automated spectral analysis methods are essential, for which methods based on iterative parametric modeling and incorporation of a priori metabolite spectral information have been widely used.[163-165] Newer algorithmic approaches using machine learning are also anticipated to play an increasing role.[166,167] Since MRSI spectra may include varying lineshapes and large lipid and unsuppressed water signals, analysis methods must include robust handling of these features. In consideration of this requirement and the typical SNR levels, the selection of simpler parametric spectral models is generally recommended; for example, while the use of a Lorentz-Gauss or variable lineshape model may be preferred for analysis of SVS data, a Gaussian lineshape may be more robust for MRSI. Similarly, inclusion of metabolite basis functions for signals with amplitudes below the detection threshold is not recommended as this will likely result in overfitting.

Spectral analysis for MRSI can benefit from application of frequency and phase corrections prior to fitting,[168,169] and from inclusion of a priori spatial information, which may include removal of local outliers or enforcing spatial smoothness of parameters. Spatial constraints can be included in the penalty function used in the optimization[170-172] or by modifying starting values for repeated applications of the spectral fitting.[164]

4.3 | Scanner integration

Considerations for integrating advanced MRSI methods into the clinical workflow include efficient processing of large datasets and combination with information derived from other imaging modalities as may be needed for several processing and analysis steps. Processing for multichannel and high-resolution volumetric MRSI acquisitions has large memory requirements, which may not be available in standard instrument configurations, and lengthy processing times, which could interfere with subsequent imaging protocols, therefore the use of automated data transfers to dedicated servers and application-specific processing programs may be required.[166,167]

5 | DATA ANALYSIS METHODS

5.1 | Quality control

Quality control is essential to reduce both false positive and false negative results. The traditional quality assessment metric, Cramer-Rao lower bounds (CRLB), needs to be used with caution, as it is only valid if the spectrum is free of artifacts and accurately described by the model used for calculation. Other measures include the fitted metabolite linewidth or the SNR; however, all of these measures would incorrectly identify as poor quality a spectrum with low metabolite content within a lesion.[173] For this situation, the linewidth measured from a coregistered water spectrum can be used, which would, for example, appropriately label necrotic regions that contain water but no measurable metabolite signals. Data-driven analysis tools can also be used to spatially segregate spectral features such as lipid contamination and baseline distortion,[174] and machine learning approaches are also anticipated to play an increasing role.[175,176]

Specific criteria for quality evaluation have not been established and can depend on the application. The commonly applied criteria for SVS, of CRLB ≤20% and linewidth ≤0.1 ppm (13 Hz at 3 T) are equally applicable to MRSI studies,[9] although these may be loosened for MRSI measurements of singlet resonances where data review will be based on visual review of metabolite images (e.g. to 15 Hz), or tightened to provide a more rigid criteria for quantitative measurements (e.g. to 11 Hz). The SNR can also be used (for nonlesional volumes only), and for quantitative measurements a minimum SNR (defined as NAA peak amplitude to RMS noise) of >10 for measurements of the primary singlet resonances or >20 for measurements of multiplet resonance groups is recommended. Depending on the disease, false negative results might be of more concern than false positive results (i.e. cancer detection), or vice versa, and quality criteria could be set to be more or less conservative with either type I or type II errors. If metabolite maps are to be used for clinical procedures, for example, neurosurgical or radiation treatment planning, it is recommended that voxels identified as being of inadequate quality be set to zero to avoid possible misinterpretation (but leaving the spectrum unchanged and available for visual review). However, for other applications it may be possible to retain all the image data, but to also display a "Quality Map" together with the metabolite maps, as illustrated in Figure 4.[135] In either situation, visual review of spectra in critical areas is still recommended.

Motion and outer volume contamination can cause artifacts that can be difficult to recognize in individual spectra or reconstructed metabolite maps, although may be better recognized as out-of-object image artifacts in maps created by spectral integration over the lipid signals. Chemical shift displacement artifacts can change spectral patterns at the edges of a volume-selected region, although this can be mitigated by improved excitation methods,[103,177] and these edge voxels should be excluded from analysis.

5.2 | Signal normalization and quantification

For comparative analyses of metabolite maps between subjects or across multiple studies, a signal normalization is required. Similar to methods used for SVS,[1,178] these may include taking metabolite ratios, ratios to tissue water, or using an external quantitation reference. Metabolite ratio maps conveniently account for bias-field intensity variations and CSF partial volume effects, and may take advantage of the complementary changes of individual metabolites, e.g. as occurs for Cho and NAA with a number of pathologies; however, precautions must be taken to prevent outliers caused by small denominator values.[179] Individual metabolite maps may also be normalized by taking the ratio to an internal reference region, e.g. from NAWM.[180] This can be done using the same metabolite, e.g. NAA/NAA_{NAWM}, or by using another metabolite as a reference, e.g. NAA/Cr_{NAWM}. These latter two approaches provide a "self-normalization" that takes into account within-subject variations, such as due to age, or changes in normal tissue associated with disease, such as brain cancer.[181,182]

For semi-quantitative single metabolite maps, both a bias-field correction (to account for transmit and receive sensitivity) and signal normalization (to account for acquisition variables) must be applied, which can be done using a coregistered proton-density MRI,[183] or a water reference MRSI.[86,184] The use of a tissue water MRSI reference has advantages

of convenience, ensuring exact coregistration and SRF, and can be used for several additional processing steps (section 3.3.3). The tissue volume fraction in each voxel can be obtained following segmentation of a high-resolution MRI and downsampled to the SRF of the MRSI study.[184,185] For truly quantitative measurements, the reference should be corrected for water content, partial volume effects, and water and metabolite relaxation times; however, these requirements, such as relaxation correction, are impractical for clinical diagnostics and results are commonly reported as institutional units to indicate that they only apply to data obtained with the identical acquisition and processing.

5.3 | Visualization and multi-modal integration

Visual inspection of individual spectra in MRSI data can be informative and frequently necessary. While system vendors provide display functionality on the MRI systems, support for interactive viewing of spectra on the PACS system is currently unavailable, which is critical for clinical integration. Support for the DICOM MRS standard[186] is also variable, with some systems using proprietary file formats or nonstandard formulations of DICOM SOP (service-object pair) classes that are incompatible with PACS. As an alternative, static DICOM secondary capture reports can be generated that show selected images and spectra, which can be sent to PACS.

Analysis of individual spectra is time-consuming and subjective, and given that advanced MRSI methods can provide metabolite maps of relatively good spatial resolution, an image review format offers clear benefits. While metabolite maps can be sent to PACS as DICOM images, these may not show sufficiently detailed anatomical structure and there is frequently missing spatial information due to FOV selection or inadequate spectral quality; therefore, additional co-localizing information from a coregistered MRI is needed. One approach is to use color-coded metabolite images overlaid on a high-resolution MRI (e.g. Figures 3 and 4), although with a caution to limit transparency to avoid overemphasizing the background MRI. A disadvantage of this approach is that the images are sent using a true color format, which does not allow further image contrast manipulation. The selection of color tables can also be problematic, particularly for metabolite ratio maps that have a very large dynamic range.

Several stand-alone MRSI display systems have been developed at research sites that provide features such as interactive spectral selection, display of spatially registered MRIs, image overlay functions and quality map information, and support for the DICOM spectroscopy standard is provided in TARQUIN,[187,188] SIVIC[189,190] and jMRUI.[191] The extension of these features into commercial medical image display packages is strongly encouraged, together with further support for the DICOM MRS standard. The development of standardized signal normalization and display methods is also recommended to increase clinical acceptance.

5.4 | Analysis methods

The combined spatial and multiparametric information of MRSI presents opportunities for novel quantitative analyses. Spatial averaging over anatomically defined regions of interest (ROIs) can be applied, either using the individual voxel fit results or by averaging the spectra

and fitting that result.[192] Voxels not meeting the quality evaluation criteria should be excluded, and for spectral summation the phase and frequency correction must be performed prior to averaging. Both methods can be extended to incorporate information on the tissue volume fraction in each voxel to separate multiple contributions such as gray and white matter.[193,194] Other examples include measurements over specific neuronal tracts,[195,196] smaller tissue regions with volume contributions from neighboring regions,[194] and different tumor regions.[197,198] ROIs can also be automatically defined using atlas registration methods, which greatly benefit from having fully 3D information to support nonlinear registration.[86,192]

The image format of MRSI naturally supports the use of voxel-based analysis (VBA) methods, which may be preferred when prior localization information is not available. An alternative to a simple calculation of a metabolite ratio map is to detect outlying values relative to a regression line generated for two metabolites, using values selected from normal tissue regions in the same subject. For example, a Cho and NAA index (CNI) has been used to highlight tumor regions (Figure 5A).[199] Comparisons between datasets from different subjects or subject groups can be performed following nonlinear spatial transform to register multiple images to a standard frame of reference where statistical tests can be carried out. This can be done for single subject data by comparing metabolite maps against mean values from a control group using a z-score analysis.[65,200] VBA methods account for normal regional variations of metabolite concentrations and any spatial variability in the reproducibility of the data; however, additional steps are needed to account for the relative tissue volume contributions,[65] and control values must be derived from a subject group that matches known covariates, notably age, while sex and body weight may also be considered.[181] The display of z-score maps greatly facilitates interpretation by directly identifying regions that are statistically different from control values (Figure 5B); however, the need for standardized acquisition methods and availability of the normative reference data make this approach difficult to translate to routine clinical studies.

The multiparametric nature of MRSI allows for multiple metabolite maps to be analyzed together, using techniques for pattern recognition analysis, as has been investigated for SVS.[201] This has primarily been done as additional image contrasts to a MRI-based tissue classification, to provide metabolic information to improve tissue classification for brain tumors.[202,203] Results indicate considerable potential for these analysis approaches; however, these methods have not been widely implemented and the requirement for consistency of imaging protocols may mean that these would be difficult to translate to clinical practice.

6 | RECOMMENDATIONS

6.1 | Acquisition methods: application-dependent selection

As described in section 3, MRSI acquisition methods offer multiple tradeoffs in terms of ease of use, acquisition times, spatial coverage and achievable spectral information. In the selection of which technique should be used, the primary considerations are the metabolic information that is needed, over what volume, and at what spatial resolution that information can be reliably obtained. The target location will also impact B_0, B_1 and lipid contamination

considerations; for example, large volume excitations would be suitable for measurements in the occipital and parietal lobes; studies of temporal lobes, where B_0 inhomogeneity is more of concern, may benefit from slice-selective excitation; and studies of the hippocampi, subcortical gray matter, or brain stem would be better sampled with 3D VOI localization methods. Considerations for acquisition variables that impact data acquisition time depend primarily on the subject group, with, for example, studies of pediatrics, advanced brain cancer, or neurodegenerative diseases benefiting from the shortest possible acquisitions (<10 minutes), whereas studies of relatively cooperative patients, as may be the case for subjects with epilepsy or migraine, may tolerate a longer examination (e.g. 12 to 20 minutes). Other considerations include available expertise, ranging from fully vendor-supported implementations that can be routinely implemented by MRI technologists to methods that require specialized expertise to ensure quality at the time of the acquisition and in the data analysis and interpretation.

Listed in Table 1 are summarized broad categories of metabolite targets, brain volumes and field strengths that correspond to different acquisition approaches, together with examples of potential clinical applications. These range from acquisition of only the primary singlet resonances, which can be reliably done at longer TEs (e.g. >50 ms), to obtaining full spectral information using short TEs with analyses of the strongly overlapping multiplet resonance patterns, and finally to the case of using specialized acquisition methods to resolve overlapping spectral compounds such as for GABA and GSH. In general, the tradeoffs of acquisition time, spatial resolution and B_0 inhomogeneity mean that smaller VOIs are more suitable if detailed spectral information is to be obtained. Therefore, the singlet resonances can be readily mapped using longer TE 3D or multi-slice MRSI over large brain volumes, without the use of spatial volume selection, whereas applications that have stricter requirements for B_0 homogeneity and robust water and subcutaneous lipid suppression, are currently best suited to volume-selected acquisitions. This last recommendation is made with consideration of the current shimming hardware and software provided by scanner manufacturers; however, following future improvements of the shim hardware/software systems, large brain volumes should also be possible for mapping of metabolites such as GABA and GSH.

The feasibility of implementing these MRSI acquisition approaches, for each of these broad categories of metabolite target groups, are summarized in Figure 6, which range from being widely available and fully integrated into available MRI systems, to requiring specialized pulse sequences and experienced personnel.

6.2 | Recommendations for minimum standards

6.2.1 | Acquisition

B_0 shimming: The biggest limiting factor and critical requirement for MRSI quality and reliability is excellent B_0 shimming. A frequency dispersion of a maximum of 20 Hz across the entire brain at 3 T should be achievable. Automated and robust B_0 shim algorithms are required[138] and further development of advanced shim hardware is strongly recommended (section 3.3.1).

Encoding and acceleration methods: Cartesian encoding methods will continue to be used for 2D or multi-slice studies but should include standard k-space undersampling options. The implementation of multi-slice and 3D SSE methods is strongly encouraged.

Motion: Incorporation of prospective motion and frequency drift correction into acquisition sequences is also highly recommended, with automatic re-shimming in case of substantial motion. Given the typical acquisition times of MRSI sequences, additional attention should be given to restricting head motion and to patient comfort.

Spatial selection: To support multiple scan protocols, several MRSI implementations are required and should include volume-selection and slice- and volume-selective localization methods, using both FID and spin-echo excitation. For volume selection the use of adiabatic excitation (e.g. semi-LASER and LASER) is recommended for ≥3 T to minimize intensity variations across the FOV[204] and chemical shift displacement.[103] For studies ≥7 T, STEAM volume selection or slice-selected FID excitation is preferred to reduce B_1 requirements and CSDE.

Water suppression: Water suppression schemes such as VAPOR or WET[205,206] that are robust against variations in transmit B_1 field intensity and T_1 relaxation times are recommended.

Extracranial lipid signals: Multiple approaches for reducing contamination from extracranial lipids should be available, including use of higher spatial resolutions and postprocessing methods. For outer volume suppression, automatic placement of multiple bands and broadband saturation pulses should be implemented.

Scanner performance: MRI systems can vary in terms of eddy currents, B_0 shimming and temporal B_0 field stability, and regular maintenance and documentation of these performance parameters is recommended.

RF performance: A minimum of 24 μT transmit field strength at 3 T is recommended for adequate performance of spectroscopy localization pulses, to limit chemical shift displacement artefacts, and to yield short TEs and adiabaticity in semi-LASER. For studies at ≥7 T, multichannel transmit is recommended and the use of spatially selective RF pulses (ie high flip angle refocusing) should be avoided to minimize CSDEs and the effects of B_1 inhomogeneities.

6.2.2 | Processing and analysis

Clinical review: Comprehensive methods for review of MRSI results on clinical PACS systems are currently not available and further commercial support for these systems is essential for clinical acceptance. Current options include transfer of metabolite maps or color-coded metabolite overlay images using standard DICOM protocols, and formation of technologist-generated static reports showing sample spectra and metabolite maps.

Image formation: A primary benefit of advanced MRSI methods is that metabolite maps can be generated with a high enough spatial resolution that image review becomes the

preferred analysis method. Relative metabolite concentrations should be derived by spectral fitting and all processing steps should be fully automated.

Individual metabolite maps should be corrected for bias-field intensity variations and signal-normalized. Current practice does not indicate a recommended normalization method and the choice is application-dependent, although preferred options include taking metabolite ratios to Cr, normalization by a reference brain region (e.g. mean value in NAWM), or as a ratio to a tissue water reference for pathologies where no change of water content may be anticipated.

Data processing: Standard spectral preprocessing methods should be used and relative metabolite concentrations should be derived by spectral fitting. Attention should be paid to maintaining performance for fitting of spectra with large baseline variations and low SNR, particularly for acquisitions involving larger FOVs. For whole-slice or whole-brain acquisitions, the use of postprocessing or specialized image reconstruction methods for reduction of extracranial lipid contamination is strongly recommended.

Quality control: Regions of poor spectral quality must be identified to avoid misinterpretation. Given the large data sizes of advanced MRSI methods, automated methods for quality control are essential; however, recognition of image artifacts can be difficult and visual review of selected voxels, particularly if indicating potential pathologies, is encouraged. It is recommended that voxels not meeting the quality criteria be set to zero value in the metabolite maps prior to clinical review, although for experienced users with access to appropriate display methods it may be preferable to keep the original metabolite images and display these together with quality maps.

Data analysis: Calculation of both metabolite ratio and individual metabolite maps is recommended, with the data used for image review being application-dependent.

For studies of brain tumors, the use of image analysis methods such as CNI maps or threshold detection of Cho/NAA maps can be used. Further development and evaluation of statistical image analysis methods for specific clinical applications are recommended.

Scanner integration: For clinical acceptance, it is essential that metabolite maps be made available shortly after acquisition. However, the combination of large data sizes and the algorithmic requirements for many image reconstruction and spectral analysis steps mean that on-scanner reconstruction for advanced MRSI methods may, in the short term, be difficult to support by the available scanner hardware, therefore dedicated computation servers may be required. Given that innovative sampling and reconstruction methods continue to be investigated, improved support for integrating custom-built reconstruction pipelines into clinical workflows needs to be provided by the system manufacturers.

Minimum MRSI display requirements must include full 3D image review capabilities with spatial coregistration with other image series, and interactive selection and display of spectra. Integration of MRSI display with interactive spectral selection into PACS systems is identified as an area where further development will be required.

7 | FUTURE DEVELOPMENT

Several ongoing technological developments will benefit future implementations of advanced MRSI methods. Continued improvements of detection sensitivity, including optimization of ultrahigh field MRI systems and improved B_1 detection and transmit array technologies, will further extend the trend to detection of an increasing number of metabolites (Figure 7) and higher spatial resolutions. This in turn leads to decreased intra-voxel B_0 inhomogeneity and a corresponding increase of the volume of the brain that can be sampled. The use of advanced shimming methods (section 3.3.1) promises to provide improved B_0 homogeneity, which together with motion correction will contribute to both greater reliability and spatial coverage. Several studies have already demonstrated that the use of higher spatial resolution acquisitions and improved reconstruction and postprocessing methods will additionally benefit sampling of cortical surface regions.[98,116,118] Further developments of under-sampled image encoding and reconstruction strategies will increase the efficiency of MRSI data collection.[116,207] With current performance providing voxel dimensions of the order of ~ 3 mm isotropic at ≥7 T for multi-slice studies (Figure 7),[98,118] when combined with high-performance volumetric spatial sampling methods, it is anticipated that comparable performance can be obtained within acquisition times from 5 to 15 minutes, depending on the FOV and resolution.

With the development of more robust B_0 shimming methods and MRSI methods that can sample a wide brain volume, the scan prescription for MRSI studies will become equivalent to any MRI method, making the acquisition methods feasible to implement in a routine clinical setting. There are also no technical barriers to providing rapid metabolite image reconstruction to provide reconstructed metabolite maps shortly after the end of the data acquisition, as is done for other clinical MRI protocols. It is anticipated that once vendor implementations of MRSI provide acquisition methods that are as easy to use as any MRI sequence, together with a full integration of the processing, then MRSI will play a greater role in clinical studies. One remaining barrier requirement will be the introduction of standardized approaches for image analysis and quality evaluation. These requirements include the development of automated and robust approaches to control for spectral quality and standardization of acquisition protocols that are matched with normal reference values to enable automated image analysis.

8 | CONCLUSION

Historically, variability in data quality, concerns with reproducibility, limitations of detection sensitivity, inefficient sampling of spatial and spectral dimensions, and limitations of review and analysis software, have held back the dissemination of MRSI. As major technological advances of MRI technologies were introduced, such as multichannel detection and transmission and higher magnetic field strengths, these have provided improvements in MRSI data quality that in turn have led to an increasing interest in clinical applications. These ongoing hardware improvements are being combined with novel spatial-spectral sampling and processing methods that provide the level of performance needed to incorporate MRSI into standardized imaging protocols. Further developments are still needed to fully integrate advanced MRSI methods into clinical studies, including robust and

automated acquisition methods, efficient processing of the large 4D datasets, and integration with PACS; however, these have largely been implemented in the research setting and there are no technical barriers to these developments. Once implemented, MRSI will become a robust image-based modality suitable for routine use. The clinical success of MRI has benefited from the high degree of automation that has been achieved and immediate presentation of the images for interpretation. Similarly, once MRSI is fully integrated as an "imaging" method it will become more widely used for routine clinical studies.

As with MRI sequences, variants of MRSI implementations are anticipated to address differing clinical requirements, with the available selection not being restricted by instrumentation performance. For this reason, this report has recommended a range of MRSI implementations that reflect the multiple tradeoffs between information content and ease of implementation. In part, these recommendations rely on continued commitment from manufacturers in implementing newer hardware and software that have been demonstrated to improve data quality.

There is ample literature demonstrating the clinical utility of MRSI, which also supports the need to translate advanced MRSI technologies into commercial products. While most of these reports of clinical value have to date been developed by the research community, a more widespread distribution of advanced MRSI technologies is now needed to support future multisite studies that will provide stronger evidence of clinical efficacy.

ACKNOWLEDGEMENTS

To the memory of Dr. Sarah Nelson, an esteemed colleague and tireless investigator of MRSI.

AAM is supported by NIH grants R01EB016064 and RO1CA172210. OCA is supported by NIH grants R01CA211080 and P50CA165962. WB is supported by the Austrian Science Fund (FWF): KLI-718, and P30701. AH is supported by European Research Council grant 679927, SYNAPLAST MR, Horizon 2020 project grant 634541, CDS-QUAMRI and CPRIT Established Researcher Recruitment grant RR180056. SJN is supported by NIH grants R01CA127612, P50CA097257 and P01CA118816. SP is supported by NIH grants 1P30GM122734 and 1R21CA241714. BJS is supported by NIH grant 1R01CA200808.

Funding information

Austrian Science Fund (FWF), Grant/Award Numbers: KLI-718, P30701; CDS-QUAMRI and CPRIT, Grant/Award Number: RR180056; European Research Council, Grant/Award Number: 679927; National Institutes of Health, Grant/Award Numbers: 1P30GM122734, 1R01CA200808, 1R21CA241714, P01CA118816, P50CA097257, P50CA165962, R01CA127612, R01CA211080, R01EB016064, RO1CA172210; SYNAPLAST MR, Horizon 2020 project grant, Grant/Award Number: 634541

Abbreviations used:

2HG	D-2-hydroxyglutarate
CRLB	Cramer-Rao lower bounds
CSDE	chemical shift displacement error
CSF	cerebrospinal fluid
DICOM	digital imaging and communications in medicine

ECC	eddy current correction
FOV	field of view
IDH	isocitrate dehydrogenase
LASER	localization by adiabatic selective refocusing
NAWM	normal-appearing white matter
OVS	outer volume suppression
PACS	picture archiving and communication system
PRESS	Point-REsolved SpectoScopy
ROI	region of interest
SIVIC	spectroscopic imaging, visualization and computing
SNR	signal-to-noise ratio
SOP	service-object pair
SRF	spatial response function
SSE	spatial-spectral encoding
STEAM	STimulated Echo Acquisition Mode
SVS	single voxel spectroscopy
VBA	voxel-based analysis
VOI	volume of interest

REFERENCES

1. Oz G, Alger JR, Barker PB, et al. Clinical proton MR spectroscopy in central nervous system disorders. Radiology. 2014;270:658–679. [PubMed: 24568703]
2. Barker PB, Bizzi A, De Stefano N, Gullapalli R, Lin DDM. Clinical MR spectroscopy: Techniques and applications. Cambridge, UK: Cambridge University Press; 2009.
3. Brown TR, Kincaid BM, Ugurbil K. NMR chemical shift imaging in three dimensions. PNAS. 1982;79:3523–3526. [PubMed: 6954498]
4. Maudsley AA, Hilal SK, Perman WH, Simon HE. Spatially resolved high-resolution spectroscopy by "four-dimensional" NMR. J Magn Reson. 1983;51: 147–152.
5. Mansfield P Spatial-mapping of the chemical-shift in NMR. J Phys D Appl Phys. 1983;16:L235–L238.
6. Ricci PE, Pitt A, Keller PJ, Coons SW, Heiserman JE. Effect of voxel position on single-voxel MR spectroscopy findings. Am J Neuroradiol. 2000;21: 367–374. [PubMed: 10696025]
7. Steffen-Smith EA, Venzon DJ, Bent RS, Hipp SJ, Warren KE. Single- and multivoxel proton spectroscopy in pediatric patients with diffuse intrinsic pontine glioma. Int J Radiat Oncol Biol Phys. 2012;84:774–779. [PubMed: 22445531]

8. Maudsley AA, Domenig C, Ramsay RE, Bowen BC. Application of volumetric MR spectroscopic imaging for localization of neocortical epilepsy. Epilepsy Res. 2010;88:127–138. [PubMed: 19926450]
9. Kreis R Issues of spectral quality in clinical 1H-magnetic resonance spectroscopy and a gallery of artifacts. NMR Biomed. 2004;17:361–381. [PubMed: 15468083]
10. Edelstein WA, Glover GH, Hardy CJ, Redington RW. The intrinsic signal-to-noise ratio in NMR imaging. Magn Reson Med. 1986;3:604–618. [PubMed: 3747821]
11. Bogner W, Gagoski B, Hess AT, et al. 3D GABA imaging with real-time motion correction, shim update and reacquisition of adiabatic spiral MRSI. Neuroimage. 2014;103:290–302. [PubMed: 25255945]
12. Zhu H, Edden RA, Ouwerkerk R, Barker PB. High resolution spectroscopic imaging of GABA at 3 Tesla. Magn Reson Med. 2011;65:603–609. [PubMed: 21337399]
13. Li Y, Larson P, Chen AP, et al. Short-echo three-dimensional H-1 MR spectroscopic imaging of patients with glioma at 7 Tesla for characterization of differences in metabolite levels. J Magn Reson Imaging. 2015;41:1332–1341. [PubMed: 24935758]
14. Li Y, Park I, Nelson SJ. Imaging tumor metabolism using in vivo magnetic resonance spectroscopy. Cancer J. 2015;21:123–128. [PubMed: 25815853]
15. Bendini M, Marton E, Feletti A, et al. Primary and metastatic intraaxial brain tumors: prospective comparison of multivoxel 2D chemical-shift imaging (CSI) proton MR spectroscopy, perfusion MRI, and histopathological findings in a group of 159 patients. Acta Neurochir. 2011;153:403–412. [PubMed: 21165751]
16. Wang Q, Zhang H, Zhang J, et al. The diagnostic performance of magnetic resonance spectroscopy in differentiating high-from low-grade gliomas: A systematic review and meta-analysis. Eur Radiol. 2016;26:2670–2684. [PubMed: 26471274]
17. Wang W, Hu Y, Lu P, et al. Evaluation of the diagnostic performance of magnetic resonance spectroscopy in brain tumors: a systematic review and meta-analysis. PLoS ONE. 2014;9:e112577. [PubMed: 25393009]
18. Usinskiene J, Ulyte A, Bjornerud A, et al. Optimal differentiation of high- and low-grade glioma and metastasis: a meta-analysis of perfusion, diffusion, and spectroscopy metrics. Neuroradiology. 2016;58:339–350. [PubMed: 26767528]
19. Dowling C, Bollen AW, Noworolski SM, et al. Preoperative proton MR spectroscopic imaging of brain tumors: correlation with histopathologic analysis of resection specimens. Am J Neuroradiol. 2001;22:604–612. [PubMed: 11290466]
20. McKnight TR, von dem Bussche MH, Vigneron DB, et al. Histopathological validation of a three-dimensional magnetic resonance spectroscopy index as a predictor of tumor presence. J Neurosurg. 2002;97:794–802. [PubMed: 12405365]
21. Chang SM, Nelson S, Vandenberg S, et al. Integration of preoperative anatomic and metabolic physiologic imaging of newly diagnosed glioma. J Neurooncol. 2009;92:401–415. [PubMed: 19357966]
22. Price SJ, Gillard JH. Imaging biomarkers of brain tumour margin and tumour invasion. Br J Radiol. 2011;84:S159–S167. [PubMed: 22433826]
23. Guo J, Yao C, Chen H, et al. The relationship between Cho/NAA and glioma metabolism: implementation for margin delineation of cerebral gliomas. Acta Neurochir. 2012;154:1361–1370. [PubMed: 22729482]
24. He T, Qiu T, Wang X, et al. Multivoxel magnetic resonance spectroscopy identifies enriched foci of cancer stem-like cells in high-grade gliomas. Onco Targets Ther. 2017;10:195–203. [PubMed: 28115854]
25. Chan AA, Lau A, Pirzkall A, et al. Proton magnetic resonance spectroscopy imaging in the evaluation of patients undergoing gamma knife surgery for Grade IV glioma. J Neurosurg. 2004;101:467–475. [PubMed: 15352605]
26. Pirzkall A, Li X, Oh J, et al. 3D MRSI for resected high-grade gliomas before RT: tumor extent according to metabolic activity in relation to MRI. Int J Radiat Oncol Biol Phys. 2004;59:126–137. [PubMed: 15093908]

27. Ballangrud AM, Lymberis S, Thakur SB, et al. Magnetic resonance spectroscopy imaging in radiotherapy planning for recurrent glioma. Med Phys. 2011;38:2724–2730. [PubMed: 21776809]
28. Einstein DB, Wessels B, Bangert B, et al. Phase II trial of radiosurgery to magnetic resonance spectroscopy-defined high-risk tumor volumes in patients with glioblastoma multiforme. Int J Radiat Oncol Biol Phys. 2012;84:668–674. [PubMed: 22445005]
29. Anwar M, Molinaro AM, Morin O, et al. Identifying voxels at risk for progression in glioblastoma based on dosimetry, physiologic and metabolic MRI. Radiat Res. 2017;188:303–313. [PubMed: 28723274]
30. Murugananandham M, Clerkin PP, Smith BJ, et al. 3-Dimensional magnetic resonance spectroscopic imaging at 3 Tesla for early response assessment of glioblastoma patients during external beam radiation therapy. Int J Radiat Oncol Biol Phys. 2014;90:181–189. [PubMed: 24986746]
31. Ken S, Vieillevigne L, Franceries X, et al. Integration method of 3D MR spectroscopy into treatment planning system for glioblastoma IMRT dose painting with integrated simultaneous boost. Radiat Oncol. 2013;8:1. [PubMed: 23280007]
32. Pirzkall A, McKnight TR, Graves EE, et al. MR-spectroscopy guided target delineation for high-grade gliomas. Int J Radiat Oncol Biol Phys. 2001;50: 915–928. [PubMed: 11429219]
33. Stadlbauer A, Moser E, Gruber S, et al. Improved delineation of brain tumors: an automated method for segmentation based on pathologic changes of 1H-MRSI metabolites in gliomas. Neuroimage. 2004;23:454–461. [PubMed: 15488395]
34. Parra NA, Maudsley AA, Gupta RK, et al. Volumetric spectroscopic imaging of glioblastoma multiforme radiation treatment volumes. Int J Radiat Oncol Biol Phys. 2014;90:376–384. [PubMed: 25066215]
35. Park I, Tamai G, Lee MC, et al. Patterns of recurrence analysis in newly diagnosed glioblastoma multiforme after three-dimensional conformal radiation therapy with respect to pre-radiation therapy magnetic resonance spectroscopic findings. Int J Radiat Oncol Biol Phys. 2007;69:381–389. [PubMed: 17513061]
36. Nelson SJ, Kadambi AK, Park I, et al. Association of early changes in 1H MRSI parameters with survival for patients with newly diagnosed glioblastoma receiving a multimodality treatment regimen. Neuro Oncol. 2017;19:430–439. [PubMed: 27576874]
37. Nelson SJ, Li Y, Lupo JM, et al. Serial analysis of 3D H-1 MRSI for patients with newly diagnosed GBM treated with combination therapy that includes bevacizumab. J Neurooncol. 2016;130:171–179. [PubMed: 27535746]
38. van Dijken BRJ, van Laar PJ, Holtman GA, van der Hoorn A. Diagnostic accuracy of magnetic resonance imaging techniques for treatment response evaluation in patients with high-grade glioma, a systematic review and meta-analysis. Eur Radiol. 2017;27:4129–4144. [PubMed: 28332014]
39. Yang I, Huh NG, Smith ZA, Han SJ, Parsa AT. Distinguishing glioma recurrence from treatment effect after radiochemotherapy and immunotherapy. Neurosurg Clin N Am. 2010;21:181–186. [PubMed: 19944976]
40. Matsusue E, Fink JR, Rockhill JK, Ogawa T, Maravilla KR. Distinction between glioma progression and post-radiation change by combined physiologic MR imaging. Neuroradiology. 2010;52:297–306. [PubMed: 19834699]
41. Sawlani V, Taylor R, Rowley K, Redfern R, Martin J, Poptani H. Magnetic resonance spectroscopy for differentiating pseudo-progression from true progression in GBM on concurrent chemoradiotherapy. Neuroradiol J. 2012;25:575–586. [PubMed: 24029093]
42. Li Y, Lupo JM, Parvataneni R, et al. Survival analysis in patients with newly diagnosed glioblastoma using pre- and postradiotherapy MR spectroscopic imaging. Neuro Oncol. 2013;15:607–617. [PubMed: 23393206]
43. Quon H, Brunet B, Alexander A, et al. Changes in serial magnetic resonance spectroscopy predict outcome in high-grade glioma during and after postoperative radiotherapy. Anticancer Res. 2011;31:3559–3565. [PubMed: 21965778]
44. Ratai EM, Zhang Z, Snyder BS, et al. Magnetic resonance spectroscopy as an early indicator of response to anti-angiogenic therapy in patients with recurrent glioblastoma: RTOG 0625/ACRIN 6677. Neuro Oncol. 2013;15:936–944. [PubMed: 23645534]

45. Cordova JS, Shu HK, Liang Z, et al. Whole-brain spectroscopic MRI biomarkers identify infiltrating margins in glioblastoma patients. Neuro Oncol. 2016;18:1180–1189. [PubMed: 26984746]
46. Trattnig S, Springer E, Bogner W, et al. Key clinical benefits of neuroimaging at 7T. Neuroimage. 2018;168:477–489. [PubMed: 27851995]
47. Li Y, Lafontaine M, Chang S, Nelson SJ. Comparison between short and long echo time magnetic resonance spectroscopic imaging at 3T and 7T for evaluating brain metabolites in patients with glioma. ACS Chem Neurosci. 2018;9:130–137. [PubMed: 29035503]
48. Li X, Vigneron DB, Cha S, et al. Relationship of MR-derived lactate, mobile lipids, and relative blood volume for gliomas in vivo. Am J Neuroradiol. 2005;26:760–769. [PubMed: 15814918]
49. Crisi G ^{1}H MR spectroscopy of meningiomas at 3.0T: the role of glutamate-glutamine complex and glutathione. Neuroradiol J. 2011;24:846–853. [PubMed: 24059885]
50. Thelwall PE, Yemin AY, Gillian TL, et al. Noninvasive in vivo detection of glutathione metabolism in tumors. Cancer Res. 2005;65:10149–10153. [PubMed: 16287997]
51. Hattingen E, Raab P, Franz K, Zanella FE, Lanfermann H, Pilatus U. Myo-inositol: a marker of reactive astrogliosis in glial tumors? NMR Biomed. 2008; 21:233–241. [PubMed: 17562554]
52. Andronesi OC, Kim GS, Gerstner E, et al. Detection of 2-hydroxyglutarate in IDH-mutated glioma patients by in vivo spectral-editing and 2D correlation magnetic resonance spectroscopy. Sci Transl Med. 2012;4:116ra4.
53. Choi C, Raisanen JM, Ganji SK, et al. Prospective longitudinal analysis of 2-hydroxyglutarate magnetic resonance spectroscopy identifies broad clinical utility for the management of patients with IDH-mutant glioma. J Clin Oncol. 2016;34:4030–4039. [PubMed: 28248126]
54. Jafari-Khouzani K, Loebel F, Bogner W, et al. Volumetric relationship between 2-hydroxyglutarate and FLAIR hyperintensity has potential implications for radiotherapy planning of mutant IDH glioma patients. Neuro Oncol. 2016;18:1569–1578. [PubMed: 27382115]
55. Andronesi OC, Loebel F, Bogner W, et al. Treatment response assessment in IDH-mutant glioma patients by noninvasive 3D functional spectroscopic mapping of 2-hydroxyglutarate. Clin Cancer Res. 2016;22:1632–1641. [PubMed: 26534967]
56. Choi C, Ganji SK, DeBerardinis RJ, et al. 2-hydroxyglutarate detection by magnetic resonance spectroscopy in IDH-mutated patients with gliomas. Nat Med. 2012;18:624–629. [PubMed: 22281806]
57. Strasser B, Gagoski B, Bijaya T, et al. Whole-brain high resolution 3D MRSI for measuring 2HG and tumor metabolism in mutant IDH glioma patients. International Society for Magnetic Resonance in Medicine, Montreal. 2019;7635.
58. An Z, Tiwari V, Baxter J, et al. 3D high-resolution imaging of 2-hydroxyglutarate in glioma patients using DRAG-EPSI at 3T in vivo. Magn Reson Med. 2019;81:795–802. [PubMed: 30277274]
59. Pan JW, Kuzniecky RI. Utility of magnetic resonance spectroscopic imaging for human epilepsy. Quant Imaging Med Surg. 2015;5:313–322. [PubMed: 25853088]
60. Mueller SG, Laxer KD, Barakos JA, et al. Metabolic characteristics of cortical malformations causing epilepsy. J Neurol. 2005;252:1082–1092. [PubMed: 15868069]
61. Pan JW, Duckrow RB, Gerrard J, et al. 7T MR spectroscopic imaging in the localization of surgical epilepsy. Epilepsia. 2013;54:1668–1678. [PubMed: 23895497]
62. Hattingen E, Luckerath C, Pellikan S, et al. Frontal and thalamic changes of GABA concentration indicate dysfunction of thalamofrontal networks in juvenile myoclonic epilepsy. Epilepsia. 2014;55:1030–1037. [PubMed: 24902613]
63. Govind V, Gold S, Kaliannan K, et al. Whole-brain proton MR spectroscopic imaging of mild-to-moderate traumatic brain injury and correlation with neuropsychological deficits. J Neurotrauma. 2010;27:483–496. [PubMed: 20201668]
64. Maudsley AA, Govind V, Levin B, Saigal G, Harris L, Sheriff S. Distributions of magnetic resonance diffusion and spectroscopy measures with traumatic brain injury. J Neurotrauma. 2015;32:1056–1063. [PubMed: 25333480]

65. Maudsley AA, Govind V, Saigal G, Gold SG, Harris L, Sheriff S. Longitudinal MR spectroscopy shows altered metabolism in traumatic brain injury. J Neuroimaging. 2017;27:562–569. [PubMed: 28736910]
66. Brown M, Baradaran H, Christos PJ, Wright D, Gupta A, Tsiouris AJ. Magnetic resonance spectroscopy abnormalities in traumatic brain injury: A meta-analysis. J Neuroradiol. 2018;45:123–129. [PubMed: 28965789]
67. Cohen BA, Inglese M, Rusinek H, Babb JS, Grossman RI, Gonen O. Proton MR spectroscopy and MRI-volumetry in mild traumatic brain injury. Am J Neuroradiol. 2007;28:907–913. [PubMed: 17494667]
68. Yeo RA, Phillips JP, Jung RE, Brown AJ, Campbell RC, Brooks WM. Magnetic resonance spectroscopy detects brain injury and predicts cognitive functioning in children with brain injuries. J Neurotrauma. 2006;23:1427–1435. [PubMed: 17020480]
69. McKee AC, Daneshvar DH. The neuropathology of traumatic brain injury. Handb Clin Neurol. 2015;127:45–66. [PubMed: 25702209]
70. Fleischer V, Kolb R, Groppa S, Zipp F, Klose U, Gröger A. Metabolic patterns in chronic multiple sclerosis lesions and normal-appearing white matter: intra-individual comparison by using 2D MR spectroscopic imaging. Radiology. 2016;281:536–543. [PubMed: 27243371]
71. Moccia M, Ciccarelli O. Molecular and metabolic imaging in multiple sclerosis. Neuroimaging Clin N Am. 2017;27:343–356. [PubMed: 28391791]
72. Heckova E, Strasser B, Hangel GJ, et al. 7 T magnetic resonance spectroscopic imaging in multiple sclerosis: How does spatial resolution affect the detectability of metabolic changes in brain lesions? Invest Radiol. 2019;54:247–254. [PubMed: 30433892]
73. Rovira A, Alonso J. 1H magnetic resonance spectroscopy in multiple sclerosis and related disorders. Neuroimaging Clin N Am. 2013;23:459–474. [PubMed: 23928200]
74. Prinsen H, de Graaf RA, Mason GF, Pelletier D, Juchem C. Reproducibility measurement of glutathione, GABA, and glutamate: Towards in vivo neurochemical profiling of multiple sclerosis with MR spectroscopy at 7T. J Magn Reson Imaging. 2017;45:187–198. [PubMed: 27351712]
75. Srinivasan R, Ratiney H, Hammond-Rosenbluth KE, Pelletier D, Nelson SJ. MR spectroscopic imaging of glutathione in the white and gray matter at 7 T with an application to multiple sclerosis. Magn Reson Imaging. 2010;28:163–170. [PubMed: 19695821]
76. Craven L, Alston CL, Taylor RW, Turnbull DM. Recent advances in mitochondrial disease. Annu Rev Genomics Hum Genet. 2017;18:257–275. [PubMed: 28415858]
77. Lin DD, Crawford TO, Barker PB. Proton MR spectroscopy in the diagnostic evaluation of suspected mitochondrial disease. Am J Neuroradiol. 2003; 24:33–41. [PubMed: 12533324]
78. Weiduschat N, Kaufmann P, Mao X, et al. Cerebral metabolic abnormalities in A3243G mitochondrial DNA mutation carriers. Neurology. 2014;82:798–805. [PubMed: 24477106]
79. Kaufmann P, Shungu DC, Sano MC, et al. Cerebral lactic acidosis correlates with neurological impairment in MELAS. Neurology. 2004;62:1297–1302. [PubMed: 15111665]
80. Quadrelli S, Mountford C, Ramadan S. Systematic review of in-vivo neuro magnetic resonance spectroscopy for the assessment of posttraumatic stress disorder. Psychiatry Res Neuroimaging. 2018;282:110–125. [PubMed: 30097168]
81. Moriguchi S, Takamiya A, Noda Y, et al. Glutamatergic neurometabolite levels in major depressive disorder: a systematic review and meta-analysis of proton magnetic resonance spectroscopy studies. Mol Psychiatry. 2018;24:952–964. [PubMed: 30315224]
82. Chandra A, Dervenoulas G, Politis M. Magnetic resonance imaging in Alzheimer's disease and mild cognitive impairment. J Neurol. 2019;266:1293–1302. [PubMed: 30120563]
83. Wang AM, Pradhan S, Coughlin JM, et al. Assessing brain metabolism with 7-T proton magnetic resonance spectroscopy in patients with first-episode psychosis. JAMA Psychiat. 2019;76:314–323.
84. Li Y, Jakary A, Gillung E, et al. Evaluating metabolites in patients with major depressive disorder who received mindfulness-based cognitive therapy and healthy controls using short echo MRSI at 7 Tesla. Magn Reson Mater Phy. 2016;29:523–533.
85. Xin L, Gambarota G, Mlynarik V, Gruetter R. Proton T-2 relaxation time of J-coupled cerebral metabolites in rat brain at 9.4T. NMR Biomed. 2008;21:396–401. [PubMed: 17907262]

86. Maudsley AA, Domenig C, Govind V, et al. Mapping of brain metabolite distributions by volumetric proton MR spectroscopic imaging (MRSI). Magn Reson Med. 2009;61:548–559. [PubMed: 19111009]
87. Posse S, DeCarli C, Le Bihan D. Three-dimensional echo-planar MR spectroscopic imaging at short echo times in the human brain. Radiology. 1994;192:733–738. [PubMed: 8058941]
88. Henning A, Fuchs A, Murdoch JB, Boesiger P. Slice-selective FID acquisition, localized by outer volume suppression (FIDLOVS) for (1)H-MRSI of the human brain at 7 T with minimal signal loss. NMR Biomed. 2009;22:683–696. [PubMed: 19259944]
89. Gruber S, Heckova E, Strasser B, et al. Mapping an extended neurochemical profile at 3 and 7 T using accelerated high-resolution proton magnetic resonance spectroscopic imaging. Invest Radiol. 2017;52:631–639. [PubMed: 28459799]
90. Boer VO, Siero JC, Hoogduin H, et al. High-field MRS of the human brain at short TE and TR. NMR Biomed. 2011;24:1081–1088. [PubMed: 21308826]
91. Chang P, Nassirpour S, Avdievitch N, Henning A. Non-water-suppressed H-1 FID-MRSI at 3T and 9.4T. Magn Reson Med. 2018;80:442–451. [PubMed: 29285781]
92. Bogner W, Gruber S, Trattnig S, Chmelik M. High-resolution mapping of human brain metabolites by free induction decay ^{1}H MRSI at 7 T. NMR Biomed. 2012;25:873–882. [PubMed: 22190245]
93. Boer VO, Klomp DW, Juchem C, Luijten PR, de Graaf RA. Multislice ^{1}H MRSI of the human brain at 7 T using dynamic B_0 and B_1 shimming. Magn Reson Med. 2012;68:662–670. [PubMed: 22162089]
94. Boer VO, van de Lindt T, Luijten PR, Klomp DW. Lipid suppression for brain MRI and MRSI by means of a dedicated crusher coil. Magn Reson Med. 2015;73:2062–2068. [PubMed: 24947343]
95. Nassirpour S, Chang P, Kirchner T. Henning A. Over-discretized SENSE reconstruction and B_0 correction for accelerated non-lipid-suppressed ^{1}H FID MRSI of the human brain at 9.4 T. NMR Biomed. 2018;31:e4014. [PubMed: 30334288]
96. Povazan M, Hangel G, Strasser B, et al. Mapping of brain macromolecules and their use for spectral processing of H-1-MRSI data with an ultra-short acquisition delay at 7 T. Neuroimage. 2015;121:126–135. [PubMed: 26210813]
97. Mullins PG, McGonigle DJ, O'Gorman RL, et al. Current practice in the use of MEGA-PRESS spectroscopy for the detection of GABA. Neuroimage. 2014;86:43–52. [PubMed: 23246994]
98. Nassirpour S, Chang P, Henning A. High and ultra-high resolution metabolite mapping of the human brain using ^{1}H FID MRSI at 9.4T. Neuroimage. 2018;168:211–221. [PubMed: 28025130]
99. Moser P, Hingerl L, Strasser B, et al. Whole-slice mapping of GABA and GABA^{+} at 7T via adiabatic MEGA-editing, real-time instability correction, and concentric circle readout. Neuroimage. 2019;184:475–489. [PubMed: 30243974]
100. Pohmann R, von Kienlin M, Haase A. Theoretical evaluation and comparison of fast chemical shift imaging methods. J Magn Reson. 1997;129: 145–160. [PubMed: 9441879]
101. Oz G, Tkac I. Short-echo, single-shot, full-intensity proton magnetic resonance spectroscopy for neurochemical profiling at 4 T: validation in the cerebellum and brainstem. Magn Reson Med. 2011;65:901–910. [PubMed: 21413056]
102. Andronesi OC, Ramadan S, Ratai EM, Jennings D, Mountford CE, Sorensen AG. Spectroscopic imaging with improved gradient modulated constant adiabaticity pulses on high-field clinical scanners. J Magn Reson. 2010;203:283–293. [PubMed: 20163975]
103. Scheenen TW, Klomp DW, Wijnen JP, Heerschap A. Short echo time 1H-MRSI of the human brain at 3T with minimal chemical shift displacement errors using adiabatic refocusing pulses. Magn Reson Med. 2008;59:1–6. [PubMed: 17969076]
104. Duyn JH, Gillen J, Sobering G, van Zijl PC, Moonen CT. Multisection proton MR spectroscopic imaging of the brain. Radiology. 1993;188:277–282. [PubMed: 8511313]
105. Osorio JA, Xu D, Cunningham CH, et al. Design of cosine modulated very selective suppression pulses for MR spectroscopic imaging at 3T. Magn Reson Med. 2009;61:533–540. [PubMed: 19097232]
106. Henning A, Schar M, Schulte RF, et al. SELOVS: brain MRSI localization based on highly selective T1- and B1- insensitive outer-volume suppression at 3T. Magn Reson Med. 2008;59:40–51. [PubMed: 18050349]

107. Spielman DM, Pauly JM, Macovski A, Glover GH, Enzmann DR. Lipid-suppressed single- and multisection proton spectroscopic imaging of the human brain. J Magn Reson Imaging. 1992;2:253–262. [PubMed: 1627859]
108. Martinez-Ramon M, Gallardo-Antolin A, Cid-Sueiro J, et al. Automatic placement of outer volume suppression slices in MR spectroscopic imaging of the human brain. Magn Reson Med. 2010;63:592–600. [PubMed: 20187173]
109. Ozhinsky E, Vigneron DB, Nelson SJ. Improved spatial coverage for brain 3D PRESS MRSI by automatic placement of outer-volume suppression saturation bands. J Magn Reson Imaging. 2011;33:792–802. [PubMed: 21448942]
110. de Graaf RA, Brown PB, De Feyter HM, McIntyre S, Nixon TW. Elliptical localization with pulsed second-order fields (ECLIPSE) for robust lipid suppression in proton MRSI. NMR Biomed. 2018;31:e3949. [PubMed: 29985532]
111. Sarkar S, Heberlein K, Hu X. Truncation artifact reduction in spectroscopic imaging using a dual-density spiral k-space trajectory. Magn Reson Imaging. 2002;20:743–757. [PubMed: 12591570]
112. Adalsteinsson E, Star-Lack J, Meyer CH, Spielman DM. Reduced spatial side lobes in chemical-shift imaging. Magn Reson Med. 1999;42:314–323. [PubMed: 10440957]
113. Zhang SH, Maier SE, Panych LP. Improved spatial localization in magnetic resonance spectroscopic imaging with two-dimensional PSF-Choice encoding. J Magn Reson. 2018;290:18–28. [PubMed: 29547794]
114. Panych LP, Roebuck JR, Chen NK, et al. Investigation of the PSF-choice method for reduced lipid contamination in prostate MR spectroscopic imaging. Magn Reson Med. 2012;68:1376–1382. [PubMed: 22648701]
115. Kirchner T, Fillmer A, Tsao J, Pruessmann KP, Henning A. Reduction of voxel bleeding in highly accelerated parallel ^{1}H MRSI by direct control of the spatial response function. Magn Reson Med. 2015;73:469–480. [PubMed: 24585512]
116. Ma C, Lam F, Ning Q, Johnson CL, Liang ZP. High-resolution 1H-MRSI of the brain using short-TE SPICE. Magn Reson Med. 2017;77:467–479. [PubMed: 26841000]
117. Klauser A, Courvoisier S, Kasten J, et al. Fast high-resolution brain metabolite mapping on a clinical 3T MRI by accelerated 1 H-FID-MRSI and low-rank constrained reconstruction. Magn Reson Med. 2019;81:2841–2857. [PubMed: 30565314]
118. Hangel G, Strasser B, Povazan M, et al. Ultra-high resolution brain metabolite mapping at 7 T by short-TR Hadamard-encoded FID-MRSI. Neuroimage. 2018;168:199–210. [PubMed: 27825954]
119. Nassirpour S, Chang P, Avdievitch N, Henning A. Compressed sensing for high-resolution nonlipid suppressed ^{1}H FID MRSI of the human brain at 9.4T. Magn Reson Med. 2018;80:2311–2325. [PubMed: 29707804]
120. Dydak U, Weiger M, Pruessmann KP, Meier D, Boesiger P. Sensitivity-encoded spectroscopic imaging. Magn Reson Med. 2001;46:713–722. [PubMed: 11590648]
121. Strasser B, Povazan M, Hangel G, et al. (2+1)D-CAIPIRINHA accelerated MR spectroscopic imaging of the brain at 7T. Magn Reson Med. 2017;78:429–440. [PubMed: 27548836]
122. Matsui S, Sekihara K, Kohno H. High-speed spatially resolved NMR spectroscopy using phase-modulated spin-echo trains. Expansion of the spectral bandwidth by combined use of delayed spin-echo trains. J Magn Reson. 1985;64:167–171.
123. Schirda CV, Zhao T, Andronesi OC, et al. In vivo brain rosette spectroscopic imaging (RSI) with LASER excitation, constant gradient strength readout, and automated LCModel quantification for all voxels. Magn Reson Med. 2016;76:380–390. [PubMed: 26308482]
124. Furuyama JK, Wilson NE, Thomas MA. Spectroscopic imaging using concentrically circular echo-planar trajectories in vivo. Magn Reson Med. 2012; 67:1515–1522. [PubMed: 22006586]
125. Lin FH, Tsai SY, Otazo R, et al. Sensitivity-encoded (SENSE) proton echo-planar spectroscopic imaging (PEPSI) in the human brain. Magn Reson Med. 2007;57:249–257. [PubMed: 17260356]
126. Larson PEZ, Bok R, Kerr AB, et al. Investigation of tumor hyperpolarized [1-C-13]-pyruvate dynamics using time-resolved multiband RF excitation echo-planar MRSI. Magn Reson Med. 2010;63:582–591. [PubMed: 20187172]

127. Zhu X, Ebel A, Ji JX, Schuff N. Spectral phase-corrected GRAPPA reconstruction of three-dimensional echo-planar spectroscopic imaging (3D-EPSI). Magn Reson Med. 2007;57:815–820. [PubMed: 17457872]
128. Tsai SY, Otazo R, Posse S, et al. Accelerated proton echo planar spectroscopic imaging (PEPSI) using GRAPPA with a 32-channel phased-array coil. Magn Reson Med. 2008;59:989–998. [PubMed: 18429025]
129. Mayer D, Kim DH, Spielman DM, Bammer R. Fast parallel spiral chemical shift imaging at 3T using iterative SENSE reconstruction. Magn Reson Med. 2008;59:891–897. [PubMed: 18383298]
130. Shankar RV, Chang JC, Hu HCH, Kodibagkar VD. Fast data acquisition techniques in magnetic resonance spectroscopic imaging. NMR Biomed. 2019;32:e4046. [PubMed: 30637822]
131. Hingerl L, Bogner W, Moser P, et al. Density-weighted concentric circle trajectories for high resolution brain magnetic resonance spectroscopic imaging at 7T. Magn Reson Med. 2018;79:2874–2885. [PubMed: 29106742]
132. Adalsteinsson E, Irarrazabal P, Topp S, Meyer C, Macovski A, Spielman DM. Volumetric spectroscopic imaging with spiral-based k-space trajectories. Magn Reson Med. 1998;39:889–898. [PubMed: 9621912]
133. Andronesi OC, Gagoski BA, Sorensen AG. Neurologic 3D MR spectroscopic imaging with low-power adiabatic pulses and fast spiral acquisition. Radiology. 2012;262:647–661. [PubMed: 22187628]
134. Li BS, Regal J, Gonen O. SNR versus resolution in 3D 1H MRS of the human brain at high magnetic fields. Magn Reson Med. 2001;46:1049–1053. [PubMed: 11746567]
135. Ebel A, Maudsley AA. Improved spectral quality for 3D MR spectroscopic imaging using a high spatial resolution acquisition strategy. Magn Reson Imaging. 2003;21:113–120. [PubMed: 12670597]
136. Gruber S, Mlynarik V, Moser E. High-resolution 3D proton spectroscopic imaging of the human brain at 3 T: SNR issues and application for anatomy-matched voxel sizes. Magn Reson Med. 2003;49:299–306. [PubMed: 12541250]
137. Sabati M, Sheriff S, Gu M, et al. Multivendor implementation and comparison of volumetric whole-brain echo-planar MR spectroscopic imaging. Magn Reson Med. 2015;74:1209–1220. [PubMed: 25354190]
138. Nassirpour S, Chang P, Fillmer A, Henning A. A comparison of optimization algorithms for localized in vivo B0 shimming. Magn Reson Med. 2018;79:1145–1156. [PubMed: 28543722]
139. Han H, Song AW, Truong TK. Integrated parallel reception, excitation, and shimming (iPRES). Magn Reson Med. 2013;70:241–247. [PubMed: 23629974]
140. Stockmann JP, Witzel T, Keil B, et al. A 32-channel combined RF and B0 shim array for 3T brain imaging. Magn Reson Med. 2016;75:441–451. [PubMed: 25689977]
141. Pan JW, Lo KM, Hetherington HP. Role of very high order and degree B0 shimming for spectroscopic imaging of the human brain at 7 Tesla. Magn Reson Med. 2012;68:1007–1017. [PubMed: 22213108]
142. Ebel A, Maudsley AA. Detection and correction of frequency instabilities for volumetric 1H echo-planar spectroscopic imaging. Magn Reson Med. 2005;53:465–469. [PubMed: 15678549]
143. Lange T, Zaitsev M, Buechert M. Correction of frequency drifts induced by gradient heating in 1H spectra using interleaved reference spectroscopy. J Magn Reson Imaging. 2011;33:748–754. [PubMed: 21563261]
144. Godenschweger F, Kagebein U, Stucht D, et al. Motion correction in MRI of the brain. Phys Med Biol. 2016;61:R32–R56. [PubMed: 26864183]
145. Posse S, Cuenod CA, Le Bihan D. Motion artifact compensation in 1H spectroscopic imaging by signal tracking. J Magn Reson B. 1993;102:222–227.
146. Hess AT, Andronesi OC, Tisdall MD, et al. Real-time motion and B0 correction for localized adiabatic selective refocusing (LASER) MRSI using echo planar imaging volumetric navigators. NMR Biomed. 2012;25:347–358. [PubMed: 21796711]

147. Posse S, Otazo R, Caprihan A, et al. Proton echo-planar spectroscopic imaging of J-coupled resonances in human brain at 3 and 4 Tesla. Magn Reson Med. 2007;58:236–244. [PubMed: 17610279]

148. Otazo R, Tsai SY, Lin FH, Posse S. Accelerated short-TE 3D proton echo-planar spectroscopic imaging using 2D-SENSE with a 32-channel array coil. Magn Reson Med. 2007;58:1107–1116. [PubMed: 17968995]

149. Zhao X, Prost RW, Li Z, Li SJ. Reduction of artifacts by optimization of the sensitivity map in sensitivity-encoded spectroscopic imaging. Magn Reson Med. 2005;53:30–34. [PubMed: 15690499]

150. Strasser B, Chmelik M, Robinson SD, et al. Coil combination of multichannel MRSI data at 7 T: MUSICAL. NMR Biomed. 2013;26:1796–1805. [PubMed: 24038331]

151. Dong Z, Peterson B. The rapid and automatic combination of proton MRSI data using multi-channel coils without water suppression. Magn Reson Imaging. 2007;25:1148–1154. [PubMed: 17905247]

152. Maril N, Lenkinski RE. An automated algorithm for combining multivoxel MRS data acquired with phased-array coils. J Magn Reson Imaging. 2005;21:317–322. [PubMed: 15723370]

153. Rodgers CT, Robson MD. Receive array magnetic resonance spectroscopy: Whitened singular value decomposition (WSVD) gives optimal Bayesian solution. Magn Reson Med. 2010;63:881–891. [PubMed: 20373389]

154. Brown MA. Time-domain combination of MR spectroscopy data acquired using phased-array coils. Magn Reson Med. 2004;52:1207–1213. [PubMed: 15508170]

155. Abdoli A, Maudsley AA. Phased-array combination for MR spectroscopic imaging using a water reference. Magn Reson Med. 2016;76:733–741. [PubMed: 26413752]

156. Haupt CI, Schuff N, Weiner MW, Maudsley AA. Removal of lipid artifacts in 1H spectroscopic imaging by data extrapolation. Magn Reson Med. 1996;35:678–687. [PubMed: 8722819]

157. Tsai SY, Lin YR, Lin HY, Lin FH. Reduction of lipid contamination in MR spectroscopy imaging using signal space projection. Magn Reson Med. 2019;81:1486–1498. [PubMed: 30277271]

158. Bilgic B, Chatnuntawech I, Fan AP, et al. Fast image reconstruction with L2-regularization. J Magn Reson Imaging. 2014;40:181–191. [PubMed: 24395184]

159. Laudadio T, Mastronardi N, Vanhamme L, Van Hecke P, Van Huffel S. Improved Lanczos algorithms for blackbox MRS data quantitation. J Magn Reson. 2002;157:292–297. [PubMed: 12323148]

160. Liu Y, Ma C, Clifford BA, et al. Improved low-rank filtering of magnetic resonance spectroscopic imaging data corrupted by noise and B_0 field inhomogeneity. IEEE Trans Biomed Eng. 2016;63:841–849. [PubMed: 26353360]

161. Zhu XP, Du AT, Jahng GH, et al. Magnetic resonance spectroscopic imaging reconstruction with deformable shape-intensity models. Magn Reson Med. 2003;50:474–482. [PubMed: 12939754]

162. Abdoli A, Stoyanova R, Maudsley AA. Denoising of MR spectroscopic imaging data using statistical selection of principal components. Magn Reson Mater Phy. 2016;29:811–822.

163. Provencher SW. Estimation of metabolite concentrations from localized in vivo proton NMR spectra. Magn Reson Med. 1993;30:672–679. [PubMed: 8139448]

164. Soher BJ, Young K, Govindaraju V, Maudsley AA. Automated spectral analysis III: Application to in vivo proton MR spectroscopy and spectroscopic imaging. Magn Reson Med. 1998;40:822–831. [PubMed: 9840826]

165. Poullet JB, Sima DM, Van Huffel S. MRS signal quantitation: a review of time- and frequency-domain methods. J Magn Reson. 2008;195:134–144. [PubMed: 18829355]

166. Bhat H, Sajja BR, Narayana PA. Fast quantification of proton magnetic resonance spectroscopic imaging with artificial neural networks. J Magn Reson. 2006;183:110–122. [PubMed: 16949319]

167. Gurbani SS, Sheriff S, Maudsley AA, Shim H, Cooper LAD. Incorporation of a spectral model in a convolutional neural network for accelerated spectral fitting. Magn Reson Med. 2019;81:3346–3357. [PubMed: 30666698]

168. Ebel A, Soher BJ, Maudsley AA. Assessment of 3D ^{1}H NMR echo-planar spectroscopic imaging using automated spectral analysis. Magn Reson Med. 2001;46:1072–1078. [PubMed: 11746571]

169. Soher BJ, Maudsley AA. Evaluation of variable line-shape models and prior information in automated 1H spectroscopic imaging analysis. Magn Reson Med. 2004;52:1246–1254. [PubMed: 15562473]

170. Kornak J, Young K, Soher BJ, Maudsley AA. Bayesian k-space-time reconstruction of MR spectroscopic imaging for enhanced resolution. IEEE Trans Med Imaging. 2010;29:1333–1350. [PubMed: 20304734]

171. Laruelo A, Chaari L, Tourneret JY, et al. Spatio-spectral regularization to improve magnetic resonance spectroscopic imaging quantification. NMR Biomed. 2016;29:918–931. [PubMed: 27166741]

172. Kelm BM, Kaster FO, Henning A, et al. Using spatial prior knowledge in the spectral fitting of MRS images. NMR Biomed. 2012;25:1–13. [PubMed: 21538636]

173. Kreis R The trouble with quality filtering based on relative Cramer-Rao lower bounds. Magn Reson Med. 2016;75:15–18. [PubMed: 25753153]

174. Ladroue C, Howe FA, Griffiths JR, Tate AR. Independent component analysis for automated decomposition of in vivo magnetic resonance spectra. Magn Reson Med. 2003;50:697–703. [PubMed: 14523954]

175. Kyathanahally SP, Doring A, Kreis R. Deep learning approaches for detection and removal of ghosting artifacts in MR spectroscopy. Magn Reson Med. 2018;80:851–863. [PubMed: 29388313]

176. Gurbani SS, Schreibmann E, Maudsley AA, et al. A convolutional neural network to filter artifacts in spectroscopic MRI. Magn Reson Med. 2018;80:1765–1775. [PubMed: 29520831]

177. McNab JA, Bartha R. Quantitative short echo-time 1H LASER-CSI in human brain at 4 T. NMR Biomed. 2006;19:999–1009. [PubMed: 16927396]

178. Jansen JF, Backes WH, Nicolay K, Kooi ME. 1H MR spectroscopy of the brain: absolute quantification of metabolites. Radiology. 2006;240:318–332. [PubMed: 16864664]

179. Maudsley AA. Lesion segmentation for MR spectroscopic imaging using the convolution difference method. Magn Reson Med. 2019;81:1499–1510. [PubMed: 30303564]

180. Elias AE, Carlos RC, Smith EA, et al. MR spectroscopy using normalized and non-normalized metabolite ratios for differentiating recurrent brain tumor from radiation injury. Acad Radiol. 2011;18:1101–1108. [PubMed: 21820634]

181. Maudsley AA, Govind V, Arheart KL. Associations of age, gender and body mass with 1H MR-observed brain metabolites and tissue distributions. NMR Biomed. 2012;25:580–593. [PubMed: 21858879]

182. Maudsley AA, Roy B, Gupta RK, et al. Association of metabolite concentrations and water diffusivity in normal appearing brain tissue with glioma grade. J Neuroimaging. 2014;24:585–589. [PubMed: 24251857]

183. Gasparovic C, Neeb H, Feis DL, et al. Quantitative spectroscopic imaging with in situ measurements of tissue water T1, T2, and density. Magn Reson Med. 2009;62:583–590. [PubMed: 19526491]

184. Gasparovic C, Song T, Devier D, et al. Use of tissue water as a concentration reference for proton spectroscopic imaging. Magn Reson Med. 2006;55:1219–1226. [PubMed: 16688703]

185. Pfefferbaum A, Adalsteinsson E, Spielman D, Sullivan EV, Lim KO. In vivo spectroscopic quantification of the N-acetyl moiety, creatine, and choline from large volumes of brain gray and white matter: Effects of normal aging. Magn Reson Med. 1999;41:276–284. [PubMed: 10080274]

186. NEMA. http://dicom.nema.org/medical/dicom/current/output/html/part03.html. Accessed August 29, 2018.

187. Wilson M, Reynolds G, Kauppinen RA, Arvanitis TN, Peet AC. A constrained least-squares approach to the automated quantitation of in vivo (1)H magnetic resonance spectroscopy data. Magn Reson Med. 2011;65:1–12. [PubMed: 20878762]

188. TARQUIN. http://tarquin.sourceforge.net. Accessed August 29, 2018.

189. Crane JC, Olson MP, Nelson SJ. SIVIC: open-source, standards-based software for DICOM MR spectroscopy workflows. Int J Biomed Imaging. 2013; 2013:169526. [PubMed: 23970895]

190. SIVIC. https://sourceforge.net/projects/sivic. Accessed August 29, 2018.

191. JMRUI. http://www.jmrui.eu. Accessed August 29, 2018.
192. Goryawala MZ, Sheriff S, Maudsley AA. Regional distributions of brain glutamate and glutamine in normal subjects. NMR Biomed. 2016;29:1108–1116. [PubMed: 27351339]
193. Hetherington HP, Pan JW, Mason GF, et al. Quantitative 1H spectroscopic imaging of human brain at 4.1 T using image segmentation. Magn Reson Med. 1996;36:21–29. [PubMed: 8795016]
194. Goryawala MZ, Sheriff S, Stoyanova R, Maudsley AA. Spectral decomposition for resolving partial volume effects in MRSI. Magn Reson Med. 2018;79:2886–2895. [PubMed: 29130515]
195. Mandl RC, van den Heuvel MP, Klomp DW, et al. Tract-based magnetic resonance spectroscopy of the cingulum bundles at 7 T. Hum Brain Mapp. 2012;33:1503–1511. [PubMed: 21674690]
196. Govind V, Sharma KR, Maudsley AA, Arheart KL, Saigal G, Sheriff S. Comprehensive evaluation of corticospinal tract metabolites in amyotrophic lateral sclerosis using whole-brain ^{1}H MR spectroscopy. PLoS ONE. 2012;7:e35607. [PubMed: 22539984]
197. Su Y, Thakur SB, Karimi S, et al. Spectrum separation resolves partial-volume effect of MRSI as demonstrated on brain tumor scans. NMR Biomed. 2008;21:1030–1042. [PubMed: 18759383]
198. Szabo de Edelenyi F, Simonetti AW, Postma G, Huo R, Buydens LMC. Application of independent component analysis to 1H MR spectroscopic imaging exams of brain tumours. Anal Chim Acta. 2005;544:36–46.
199. McKnight TR, Noworolski SM, Vigneron DB, Nelson SJ. An automated technique for the quantitative assessment of 3D-MRSI data from patients with glioma. J Magn Reson Imaging. 2001;13:167–177. [PubMed: 11169821]
200. Signorini M, Paulesu E, Friston K, et al. Rapid assessment of regional cerebral metabolic abnormalities in single subjects with quantitative and non-quantitative [18F]FDG PET: A clinical validation of statistical parametric mapping. Neuroimage. 1999;9:63–80. [PubMed: 9918728]
201. Perez-Ruiz A, Julia-Sape M, Mercadal G, et al. The INTERPRET decision-support system version 3.0 for evaluation of magnetic resonance spectroscopy data from human brain tumours and other abnormal brain masses. BMC Bioinformatics. 2011;11:581.
202. De Edelenyi FS, Rubin C, Estève F, et al. A new approach for analyzing proton magnetic resonance spectroscopic images of brain tumors: nosologic images. NatMed. 2000;6:1287–1289.
203. Raschke F, Barrick TR, Jones TL, Yang G, Ye X, Howe FA. Tissue-type mapping of gliomas. Neuroimage Clin. 2019;21:101648. [PubMed: 30630760]
204. Wilson M, Andronesi OC, Barker PB, et al. A methodological consensus on clinical proton MR spectroscopy of the brain: review and recommendations. Magn Reson Med. 2019;82:527–550. [PubMed: 30919510]
205. Tkac I, Starcuk Z, Choi IY, Gruetter R. In vivo 1H NMR spectroscopy of rat brain at 1 ms echo time. Magn Reson Med. 1999;41:649–656. [PubMed: 10332839]
206. Ogg RJ, Kingsley PB, Taylor JS. WET, a T1-and B1-intensive water-suppression method for in vivo localized 1H NMR spectroscopy. J Magn Reson. 1994;104:1–10.
207. Cao P, Shin PJ, Park I, et al. Accelerated high-bandwidth MR spectroscopic imaging using compressed sensing. Magn Reson Med. 2016;76:369–379. [PubMed: 27228088]
208. Hingerl L, Strasser B, Moser P, et al. Towards full-brain FID-MRSI at 7T with 3D concentric circle readout trajectories. International Society for Magnetic Resonance in Medicine, Toronto, 2019; 618.
209. Magnusson PO, Boer VO, Marsman A, et al. Gamma-aminobutyric acid edited echo-planar spectroscopic imaging (EPSI) with MEGA-sLASER at 7T. Magn Reson Med. 2018;81:773–780. [PubMed: 30159924]

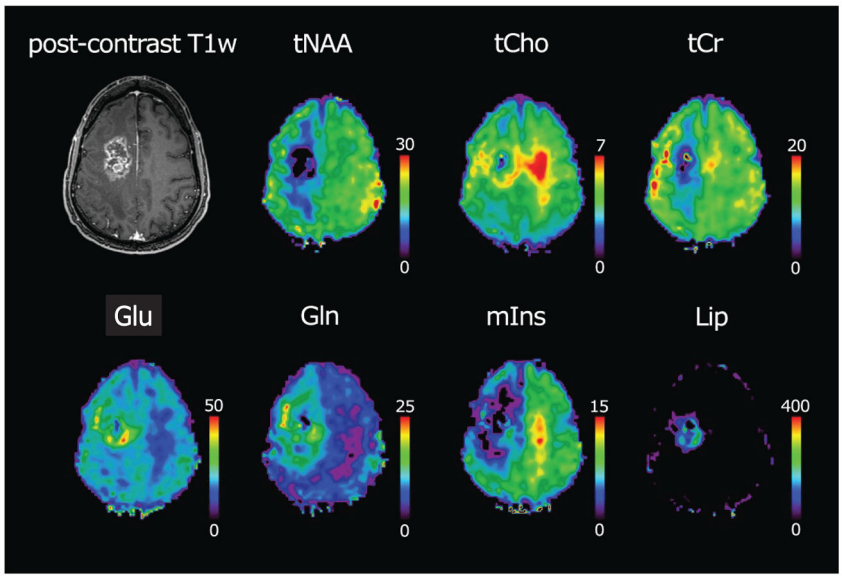

FIGURE 1.

MRSI obtained at 7 T for a subject with an anaplastic oligoastrocytoma. Shown are the T1-weighted postcontrast MRI, total N-acetylaspartate (tNAA), total choline (tCho), total creatine (tCr), glutamate (Glu), glutamine (Gln), myo-inositol (mIns) and sum of lipids (Lip). The single-slice FID-MRSI was acquired in 6 min with 6-fold accelerated phase-encoding, voxel size of 3.4 x 3.4 x 8 mm^3 and TR/AD of 600/1.3 ms. From Trattnig et al[46]

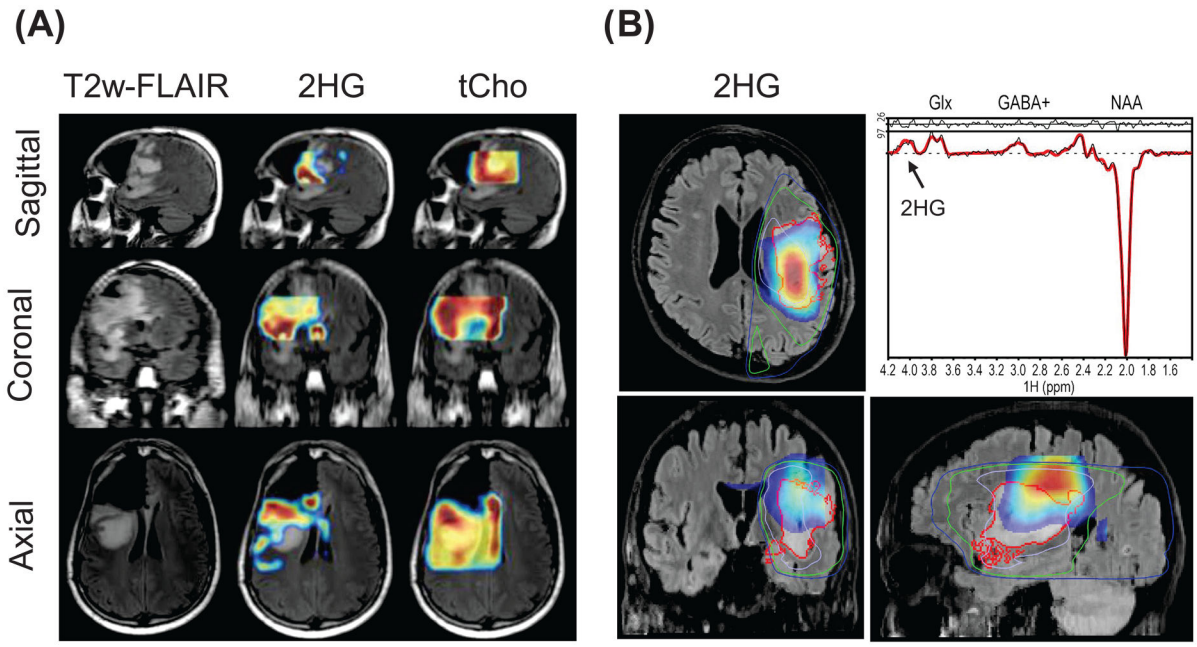

FIGURE 2.

Volumetric MRSI measurements of 2HG at 3 T. (A) 2HG maps for a glioblastoma, postsurgery. Maps were obtained using PRESS at TE = 97 ms with 3D phase encoding and are superimposed on the FLAIR MRI. From Choi C et al.[58] (B) 2HG maps for a glioblastoma obtained using an editing measurement based on MEGA-LASER at TE = 68 ms and 3D stack-of-spirals. The red contours indicate the tumor margins on FLAIR image while the blue and green contours show the radiotherapy dose. From Jafari-Khouzani et al[54]

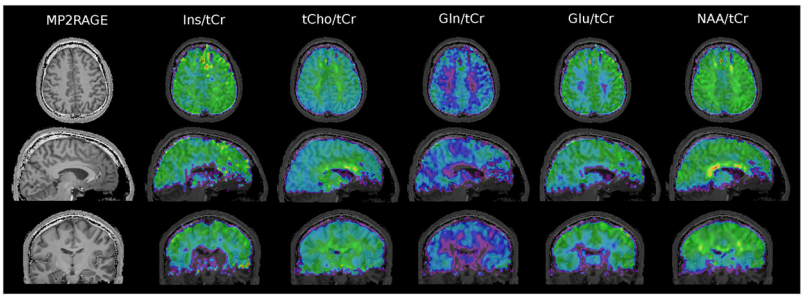

FIGURE 3.

Whole-brain high-resolution metabolite maps taken at 7 T using FID-detection (acquisition delay 1.3 ms, TR = 280 ms), concentric-ring k-space sampling and reconstruction to 80 x 80 x 47 voxels. Total acquisition time was 15 minutes. Additional details can be found in Hingerl et al[208]

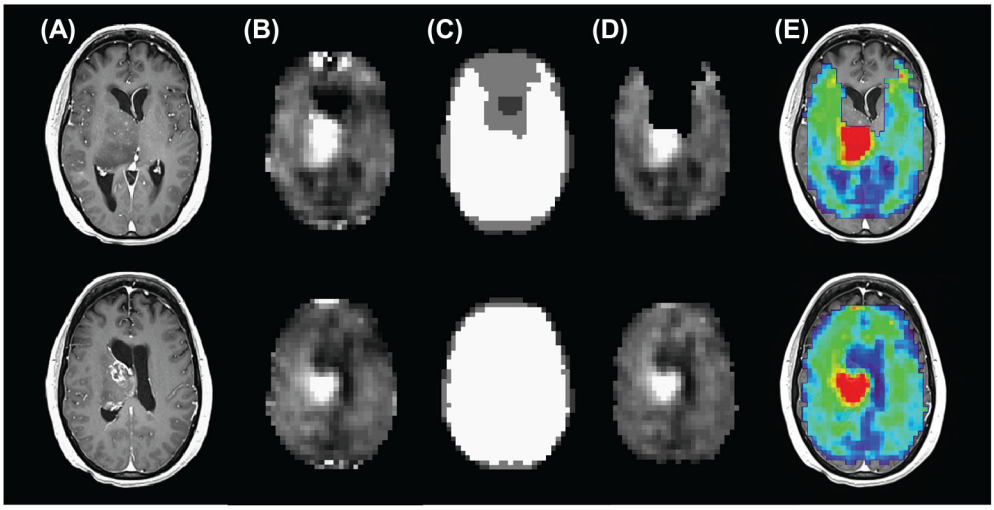

FIGURE 4.

Example of the use of quality maps to identify regions with spectra of inadequate quality, for two slices from a volumetric EPSI acquisition at 3 T, for TE = 50 ms. Shown are (A) the postcontrast T1-weighted MRI and (B) the Cho map, which shows increased signal corresponding to the location of a glioblastoma, together with several other bright signal regions. In (C) are shown the spectral quality maps, with white regions corresponding to a spectral linewidth of ≤13 Hz and gray regions for voxels with a linewidth of >13 Hz. Poor quality voxels can be removed (D), although spatial information is more clearly conveyed when combined as an overlay image with the MRI (E)

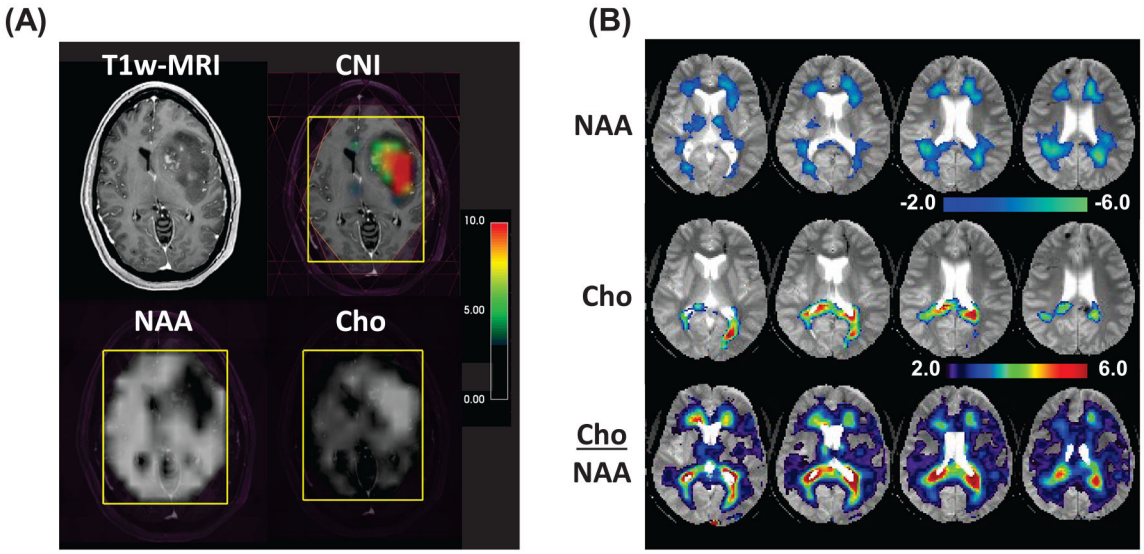

FIGURE 5.

(A) Example volume-selected 3 T MRSI result for a glioblastoma showing the contrast-T1 MRI, the Choline-to-NAA Index (CNI) map, and the NAA and Cho metabolite maps. The selected volume is indicated by the yellow rectangle. The CNI map, shown as a color overlay, identifies all voxels with significant differences of the ratio of NAA and Cho. The color bar represents the numerical values of the CNI map. (B) Example Z-score maps for NAA, Cho and Cho/NAA at a time point of 1.7 months following a traumatic brain injury of moderate severity (Glasgow Coma Score 13). The color overlays represent the significance of the difference for the single subject values relative to mean values from an age-matched control group of 25 subjects, with decreased value for NAA and increased values for Cho and Cho/NAA. Adapted from Maudsley et al[65]

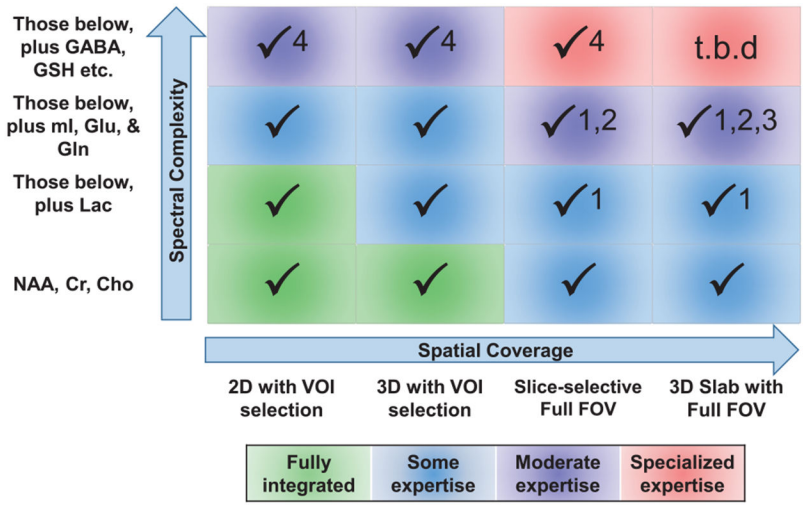

FIGURE 6.

Illustration of the recommended classes of acquisition methods for increasing levels of complexity of the spectral information. The color indicates the level of expertise required, ranging from sequences that are fully integrated into clinical protocols to specialized sequences that require specific research experience. Observations indicated by the numbers are as follows: (1) whole-brain acquisitions are susceptible to increased contamination from extracranial lipids; therefore, results from spectral fitting of lactate are labeled LL (Lipid +Lactate). (2) Whole-slice or whole-brain acquisitions benefit from using higher spatial resolutions[92,118,135] and are therefore not optimum for detection of low SNR signal components for ≤3T measurements. (3) Whole-brain acquisitions have large global B_0 inhomogeneities and quantitative analysis of resonances close to water and lipid may be impacted in some brain regions. (4) Measurements of compounds that have significant spectral overlap are widely implemented using frequency-spectral editing methods, which are most reliably implemented using volume-selective measurements[11,12,209]

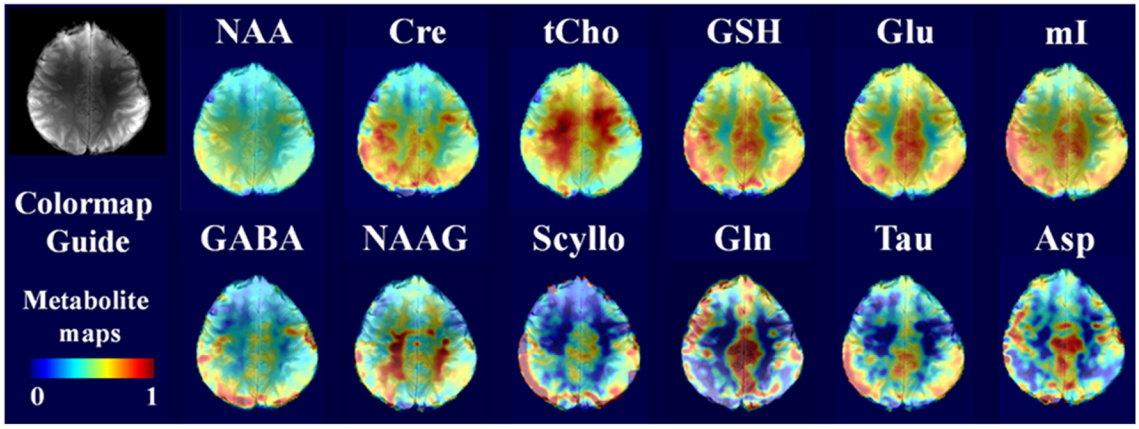

FIGURE 7.

Single slice (top) and whole brain multi-slice (bottom) ^{1}H FID MRSI acquired at 9.4 T. Scan time was 11 minutes for one slice (TR = 220 ms, 3.1 x 3.1 x 10 mm) and 25 minutes for the whole-brain scan (TR = 300 ms, 10 slices, 3.2 x 3.2 x 8mm, 7-fold acceleration). Modified from Nassirpour et al[98]

TABLE 1

Broad categories for groups of metabolites and brain volumes over which they can be detected at different field strengths and example clinical applications. Metabolites marked with an asterisk are best observed at ≥7T

Target metabolites	Methods	Field strength	Example clinical applications
NAA, Cr, Cho	Long TE, large FOV 3D volume	1.5 and 3 T	• Brain tumor treatment planning, biopsy guidance • Neocortical epilepsy localization • Traumatic brain injury
NAA, Cr, Cho, Lac	Long TE, 3D volume with suppression of subcutaneous lipids	1.5 and 3 T	• Mitochondrial disorders • Chronic fatigue • Brain tumor evaluation
NAA, Cr, Cho, Glu, Gln, mI, Lac	Short TE, volume-selected 2D or 3D	All	• Psychiatric disorders • Neurodegenerative diseases • Brain tumor grading • Abscess vs. primary tumor and necrosis
GABA, GSH, 2HG, etc.	Spectral editing with volume-selected 2D	3 and 7 T	• Psychiatric disorders • Studies on aging • Studies on pain • Brain tumor diagnosis • Brain tumor treatment planning (e.g. 2HG)
NAA, Cr, Cho, Glu, mI, Gln*, NAAG*, GSH*, GABA*	FID, 2D (multi) slice or 3D volume with high spatial resolution	3, 7 and 9.4 T	• MS • Epilepsy • Neurodegenerative diseases • Psychiatric disorders